NAVAL POSTGRADUATE SCHOOL

MONTEREY, CALIFORNIA

THESIS

LIDAR AND IMAGE POINT CLOUD COMPARISON

by

Amanda R. Mueller

September 2014

Thesis Advisor:	Richard C. Olsen
Second Reader:	David M. Trask

Approved for public release; distribution is unlimited

THIS PAGE INTENTIONALLY LEFT BLANK

REPORT DOCUMENTATION PAGE		*Form Approved OMB No. 0704-0188*

Public reporting burden for this collection of information is estimated to average 1 hour per response, including the time for reviewing instruction, searching existing data sources, gathering and maintaining the data needed, and completing and reviewing the collection of information. Send comments regarding this burden estimate or any other aspect of this collection of information, including suggestions for reducing this burden, to Washington headquarters Services, Directorate for Information Operations and Reports, 1215 Jefferson Davis Highway, Suite 1204, Arlington, VA 22202-4302, and to the Office of Management and Budget, Paperwork Reduction Project (0704-0188) Washington DC 20503.

1. AGENCY USE ONLY *(Leave blank)*	2. REPORT DATE September 2014	3. REPORT TYPE AND DATES COVERED Master's Thesis	
4. TITLE AND SUBTITLE LIDAR AND IMAGE POINT CLOUD COMPARISON		5. FUNDING NUMBERS	
6. AUTHOR Amanda R. Mueller			
7. PERFORMING ORGANIZATION NAME(S) AND ADDRESS(ES) Naval Postgraduate School Monterey, CA 93943-5000		8. PERFORMING ORGANIZATION REPORT NUMBER	
9. SPONSORING /MONITORING AGENCY NAME(S) AND ADDRESS(ES) N/A		10. SPONSORING/MONITORING AGENCY REPORT NUMBER	
11. SUPPLEMENTARY NOTES The views expressed in this thesis are those of the author and do not reflect the official policy or position of the Department of Defense or the U.S. Government. IRB protocol number ____N/A____.			
12a. DISTRIBUTION / AVAILABILITY STATEMENT Approved for public release; distribution is unlimited		12b. DISTRIBUTION CODE A	

13. ABSTRACT (maximum 200 words)

This paper analyzes new techniques used to extract 3D point clouds from airborne and satellite electro-optical data. The objective of this research was to compare the three types of point clouds to determine whether image point clouds could compete with the accuracy of LiDAR point clouds. The two main types of image point clouds are those created photogrammetrically, with two side-by-side images, or through feature matching between multiple images using multiview stereo techniques. Two software packages known for handling aerial imagery, IMAGINE Photogrammetry and Agisoft Photoscan Pro, were used to create such models. They were also tested with sub-meter resolution satellite imagery to determine whether much larger, but still truthful, models could be produced. It was found that neither software package is equipped to vertically analyze satellite imagery but both were successful when applied to aerial imagery. The photogrammetry model contained fewer points than the multiview model but maintained building shape better. While the photogrammetry model was determined to be the more accurate of the two it still did not compare to the accuracy of the LiDAR data.

14. SUBJECT TERMS LiDAR, photogrammetry, multiview stereo, point cloud			15. NUMBER OF PAGES 83
			16. PRICE CODE
17. SECURITY CLASSIFICATION OF REPORT Unclassified	18. SECURITY CLASSIFICATION OF THIS PAGE Unclassified	19. SECURITY CLASSIFICATION OF ABSTRACT Unclassified	20. LIMITATION OF ABSTRACT UU

THIS PAGE INTENTIONALLY LEFT BLANK

LIDAR AND IMAGE POINT CLOUD COMPARISON

Amanda R. Mueller
Second Lieutenant, United States Air Force
B.S., United States Air Force Academy, 2013

Submitted in partial fulfillment of the
requirements for the degree of

MASTER OF SCIENCE IN REMOTE SENSING INTELLIGENCE

from the

NAVAL POSTGRADUATE SCHOOL
September 2014

Author: Amanda R. Mueller

Approved by: Richard C. Olsen
                   Thesis Advisor

                   David M. Trask
                   Second Reader

                   Dan C. Boger
                   Chair, Department of Information Science

THIS PAGE INTENTIONALLY LEFT BLANK

ABSTRACT

This paper analyzes new techniques used to extract 3D point clouds from airborne and satellite electro-optical data. The objective of this research was to compare the three types of point clouds to determine whether image point clouds could compete with the accuracy of LiDAR point clouds. The two main types of image point clouds are those created photogrammetrically, with two side-by-side images, or through feature matching between multiple images using multiview stereo techniques. Two software packages known for handling aerial imagery, IMAGINE Photogrammetry and Agisoft Photoscan Pro, were used to create such models. They were also tested with sub-meter resolution satellite imagery to determine whether much larger, but still truthful, models could be produced. It was found that neither software package is equipped to vertically analyze satellite imagery but both were successful when applied to aerial imagery. The photogrammetry model contained fewer points than the multiview model but maintained building shape better. While the photogrammetry model was determined to be the more accurate of the two it still did not compare to the accuracy of the LiDAR data.

THIS PAGE INTENTIONALLY LEFT BLANK

TABLE OF CONTENTS

THIS PAGE INTENTIONALLY LEFT BLANK

LIST OF FIGURES

LIST OF TABLES

THIS PAGE INTENTIONALLY LEFT BLANK

LIST OF ACRONYMS AND ABBREVIATIONS

2D	2-dimensional
2.5D	2.5-dimensional
3D	3-dimensional
CC	CloudCompare
DEM	digital elevation model
DSM	digital surface model
ETS	electronic total station
GCP	ground control point
GPS	Global Positioning System
IMU	inertial measurements unit
LiDAR	light detection and ranging
MI	mutual information
MVS	multiview stereo
PRF	pulse repetition frequency
QTM	Quick Terrain Modeler
SfM	structure from motion
TIN	triangular irregular network
TOF	time of flight
UAV	unmanned aerial vehicle
USGS	United States Geological Survey
UTM	Universal Transverse Mercator
WGS 84	World Geodetic System 1984
WSI	Watershed Sciences, Inc.

THIS PAGE INTENTIONALLY LEFT BLANK

ACKNOWLEDGMENTS

THIS PAGE INTENTIONALLY LEFT BLANK

I.   INTRODUCTION

A.   PURPOSE OF RESEARCH

Light detection and ranging (LiDAR) is a remote sensing technology that has bloomed in the last 30 years. It transmits pulses of light toward an object and collects the returns in order to create a 3-dimensional (3D) model called a point cloud. When taken from an airplane digital surface models (DSMs) can be created to accurately map objects on the Earth's surface or objects can be removed to create digital elevation models (DEMs) of the surface itself. These DEMs can be used to make topographic maps because they reveal changes in elevation.

Photogrammetry, the science of making 3D models by making measurements on side-by-side photographs, existed well before LiDAR. The technology has been updated to the point that pixels in digital images can be registered to create point clouds.

Recent progress in computer vision technology has brought forth a competing method for creating 3D models: multiview stereopsis (MVS). MVS programs use photographs taken of an object or scene from multiple different angles to recreate a point cloud likeness of the original in 3D space. By matching unique features in each photograph and determining from which direction the images were taken, accurate models can be built of the entire scene.

This research will compare the point clouds produced in all three methods to demonstrate the possibility of using the imagery techniques in place of LiDAR.

B.   OBJECTIVE

The objective of this research is to demonstrate the accuracy of photogrammetric and MVS point cloud models as compared to LiDAR-derived point cloud models. Point clouds of each of the datasets were compared to establish the usability of the imagery techniques.

THIS PAGE INTENTIONALLY LEFT BLANK

II.   BACKGROUND

Two very different communities have contributed to the evolution of today's MVS techniques: photogrammetrists with their exact science of measuring image distances and computer visionaries with their pursuit of automated image matching. LiDAR shares a parent discipline with photogrammetry, having been developed within the surveying community, but it has since branched out to airborne and spaceborne activities over the past two decades.

A.   PHOTOGRAMMETRY

The art of photogrammetry was born in 1851, when Colonel Aimé Laussedat, the "Father of Photogrammetry," of the French Corps of Engineers began tinkering with measurements taken from photographs in hopes of working out a model for creating topographic maps without the extreme amount of manual labor required to survey large areas.

After 10 years, in 1861, Laussedat was able to create the "Plan of the Village of Buc, near Versailles" using terrestrial images, seen in Figure 1 (Aerial, 2013). In the top right corner, two vertices reveal multiple angles of interest used in the drawing of this plan, representing the camera locations at the time each photograph was taken. These positions indicate hilltops or tall towers from which many details of the village would have been visible.
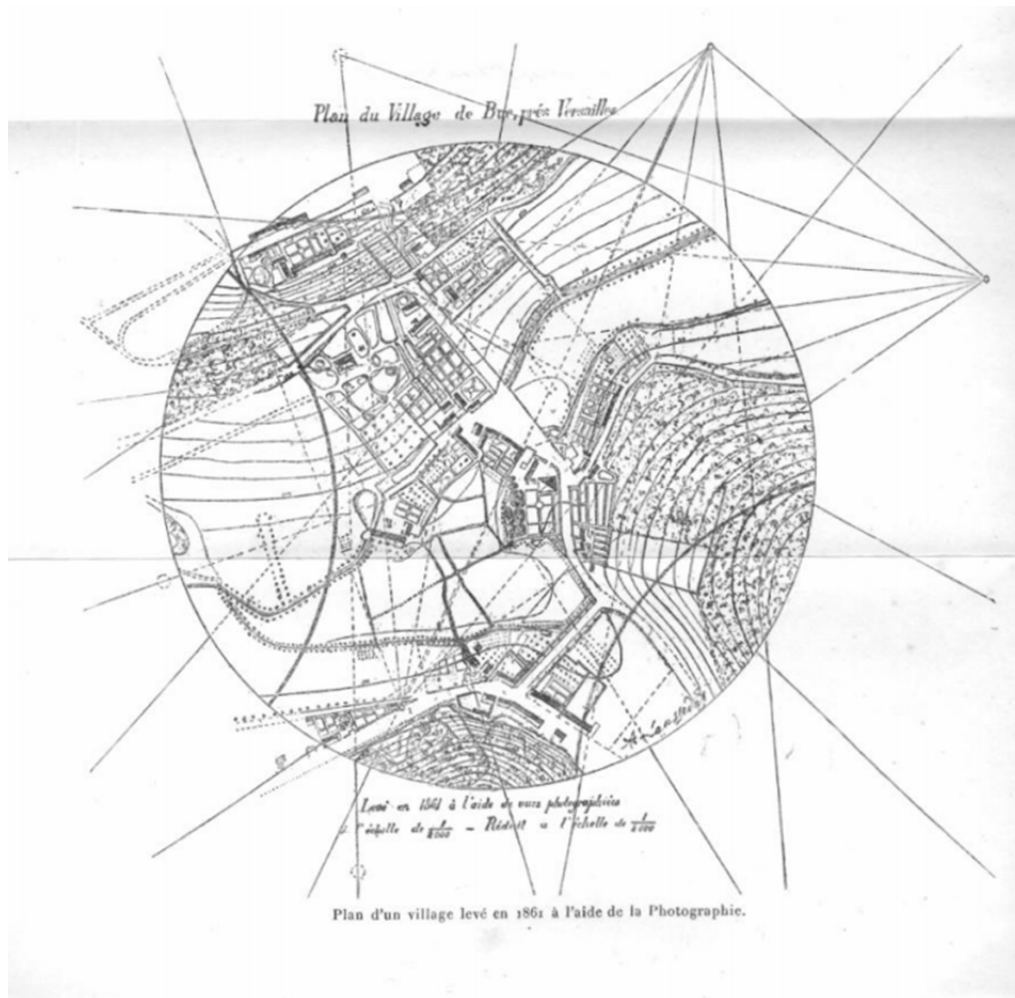
Figure 1.   "Plan of the Village of Buc, near Versailles" Created by Aimé
Laussedat in 1861 (from Laussedat, 1899, p. 54)

In addition to this work, Laussedat attempted to use photographs taken from kites and rooftops. In 1858, he experimented with the famous French photographer Nadar on utilizing the wet collodion process to take photographs from hot air balloons. As seen in Figure 2, it was necessary to take two images of the same location from slightly different angles in order to determine object heights. By the Paris Exposition of 1867, he was ready to present a map of Paris based on photographic surveys. Laussedat's map closely matched earlier instrument surveys and his technique was examined and found satisfactory by two members of the Academie des Sciences ("Laussedat," 2008).

Figure 2.   Hot Air Balloon Photography of Paris taken by Gaspard-Felix
                 Tournachon, Better Known as Nadar (from Saiz, 2012)

This work was made possible by the invention of photography in 1839, as well as contributions to mathematical perspective by Brooke Taylor in 1715 and Johann Heinrich Lambert in 1759 and to advances in nautical surveying by Charles-Francois Beautemps-Beaupre in 1791 (Church, 1948). Laussedat's work spurred the development of many kinds of ground photographic equipment such as a photographic plane-table, panoramic apparatus, the photo-theolodite, and the photogoniometer. Over time, the quality of lenses, photographic material, and recording devices also improved to the point that cameras could be attached to kites and balloons, and eventually flown on dirigibles and airplanes.

Thomas Scheimpflug was an Austrian naval officer who pursued kite-borne photography because he was disillusioned by the amount of time it took to create maps during the late 1800s. Inspired by his practical geometry teacher's explanation of how the

new science of photogrammetry was much faster than manual point-to-point image correlation young Thomas set forth to develop the "photo karte," a distortion-free photograph that could be used to make highly accurate maps (Erdkamp, 2011). Utilizing ideas from a 1901 British patent submitted by Parisian engineer, Jules Carpentier, he was able to submit his own patent in 1904 describing an apparatus to alter or (un)distort photographs (Merklinger, 1996). In this work, he described what would later become known as the "Scheimpflug principle," named for him not because he invented it but because he strongly promoted it, which outlines how a camera's lens and back should be positioned when trying to focus on a plane that is not parallel to the film. Figure 3 demonstrates this idea: A is the film plane, B is the plane passing through the lens and C is the plane of sharp focus through the object. Both A and B may need to be adjusted to ensure all three intersect.
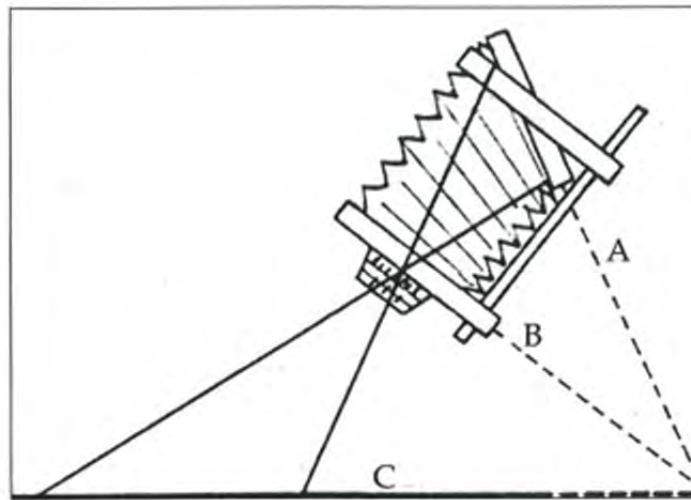
Figure 3.   Schematic of the Scheimpflug Principle (from Erdkamp, 2011)

The Scheimpflug principle is vital to aerial photography and led to Scheimpflug's passion for panoramic cameras. Aerial surveys at the time required photographs that covered large areas of land in order to ensure they contained points of a triangulation web laid by surveyors. Stereopairs were also necessary for determining contour lines. Scheimpflug tested 7- and 8-lens cameras by attaching them to kites because the

multitude of angles provided more than 100-degree views of the ground. His most popular camera configurations are shown in Figure 4.
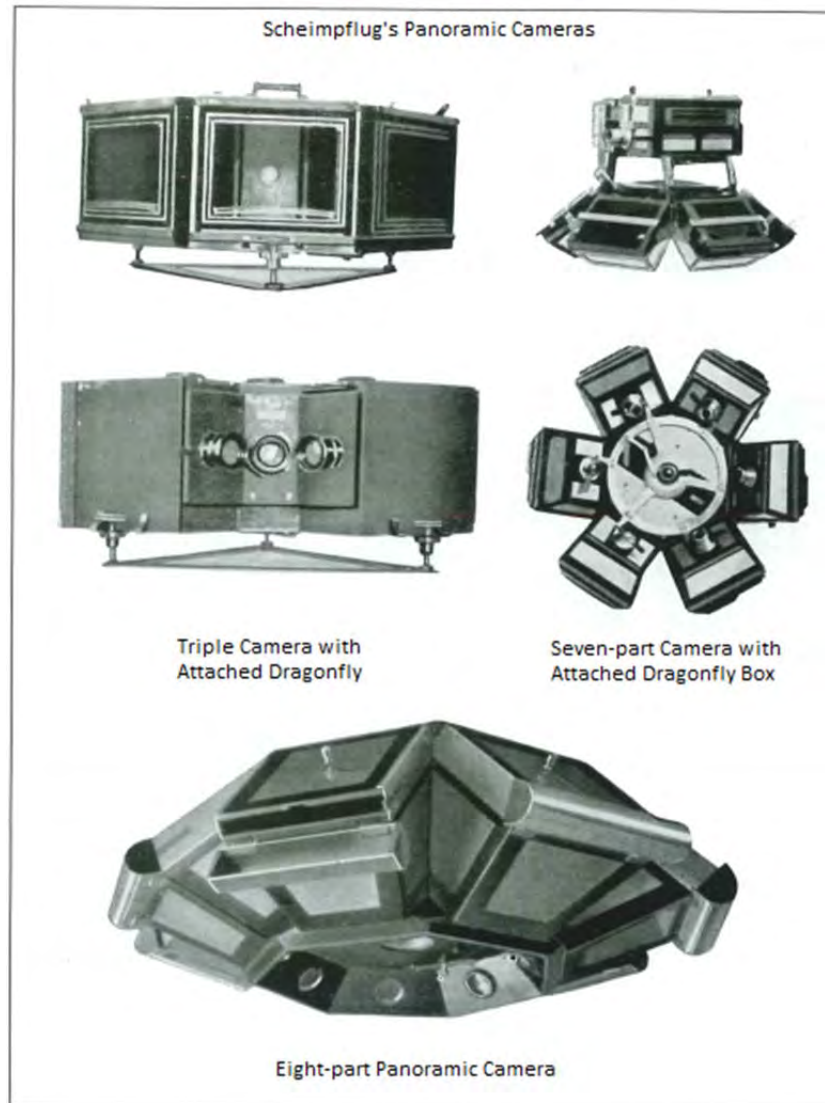
Figure 4.   Scheimpflug's Camera Configurations (from Erdkamp, 2011)

For the actual map-making one more piece of equipment was needed: the "photo perspektograph" camera. This device, seen in Figure 5, processed aerial photographs to remove distortion by compensating for the decrease in scale proportional to the distance from the camera. This distorting enlarger corrected object proportions and positioned

them where they ought to be on a conventional map (Erdkamp, 2011). Finally, maps could be made directly from corrected photographs.
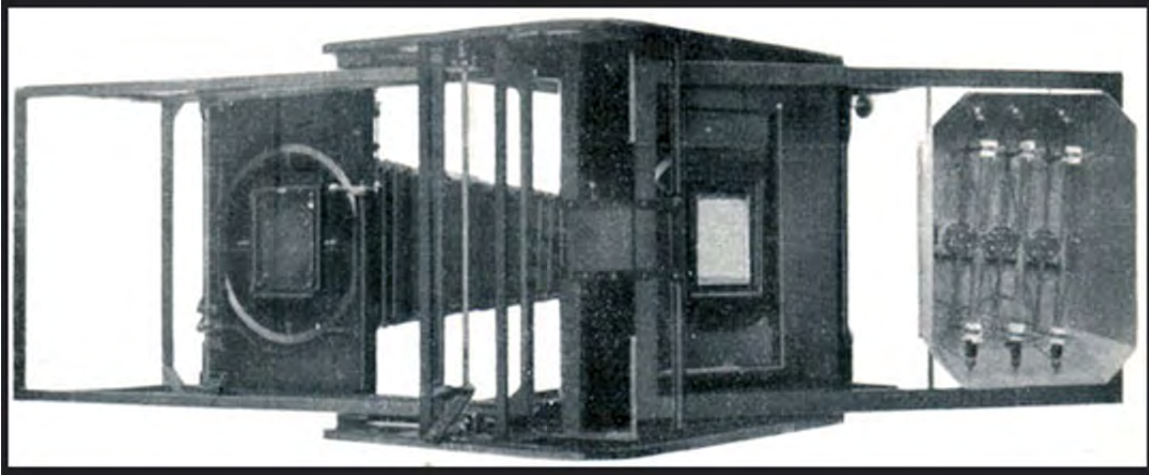
Figure 5.   Scheimpflug's Photo Perspektograph Model II (from Erdkamp, 2011)

Captain Cesare Tardivo was as dedicated to aerial imagery and surveying as Thomas Scheimpflug. After many years of working with hot air balloons as a member of the Photographic Section of the Italian Specialist Brigade, Tardivo was able to present surveys, such as the one seen in Figure 6, to the International Conference of Photography (Guerra & Pilot, 2000). The success of this topographic survey of Ostia (Antica), the location of ancient Rome's harbor city, finished in 1911, helped convince military and civilian groups of the utility of this new discipline.

Figure 6.   Topographic Survey of Ostia from a Hot Air Balloon
(from Shepherd, 2006)

As support and interest grew, Tardivo wrote a book on the subject. His "Manual of Photography, Telephotography, and Topography from Balloon" explains many aspects of surveying, from appropriate weather conditions and the dimensions required for a balloon to carry certain instruments to the need of having a tailor on the collection team in case of repairs (1911). As inferred from in Figure 7, large numbers of images were required in order to cover any sizable area because only the centers of each photograph were geometrically correct enough for use in maps, and successive images were rarely aligned. With the invention of the airplane in 1903 this changed drastically because images could be collected quickly and efficiently, following pre-planned flight paths in controlled directions.
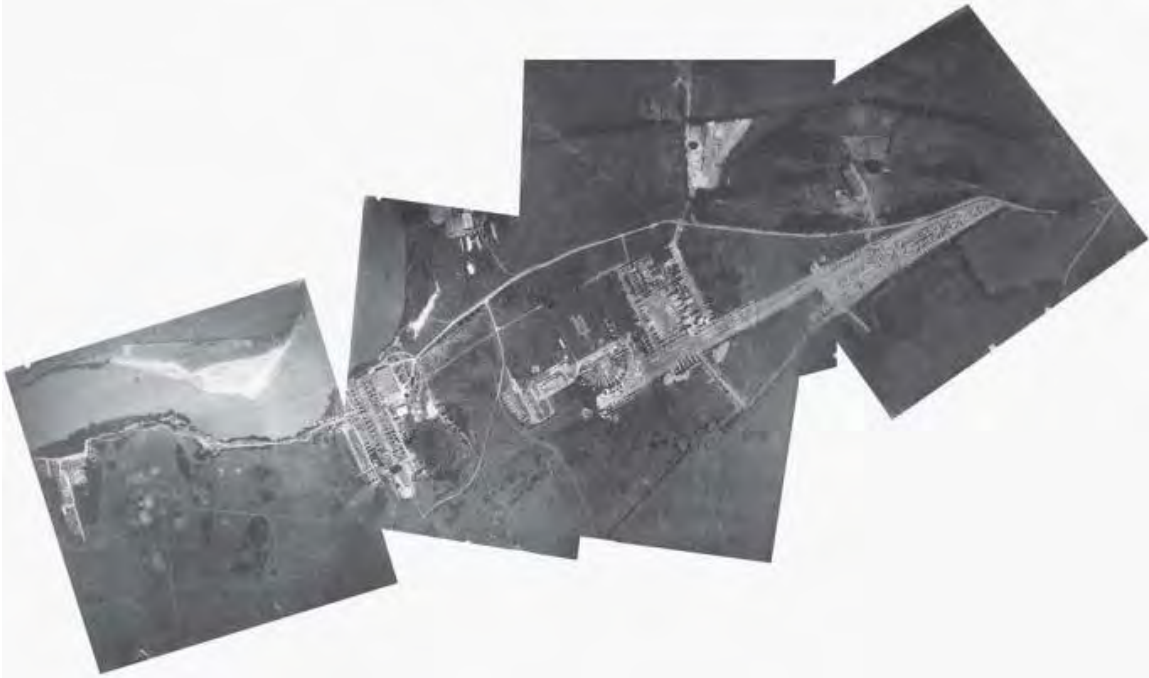
Figure 7.   Mosaic of Images Taken of Ostia For Use in the Topographic Survey
by Hot Air Balloon (from Shepherd, 2006)

In the United States, terrestrial photographs were first used for topographic mapping in 1904 when a panoramic camera was taken to Alaska by the United States Geological Survey (USGS) (Church, 1948). Topographic maps depict terrain in three dimensions with the topographic relief usually represented by contour lines. James Bagley documented and later published much of what he learned firsthand about terrestrial surveying and applying photogrammetry to aerial surveys (1917). He and another member of the USGS team to Alaska, F. H. Moffitt, were inspired to build a three-lens camera, as seen in Figure 8, based on the cameras of Thomas Scheimpflug.

Figure 8.   Three-Lens Camera Used by USGS Team in Alaska, with One
Vertical and Two Obliques (from "Early Techniques," 2000)

The T-1, their tri-lens camera built in 1916, had "one lens pointing vertically downward and two lenses inclined 35 degrees from the vertical" (Church, 1948). This setup allowed crews to collect photographs of a flight path from three separate angles on a single pass. This three-lens method created less distortion than the wide angle lenses that were popular at the time. As World War I progressed, Bagley was sent to France to continue work on the tri-lens camera and after the war he stayed on with the Army at McCook Field. Advances made over the next 25 years proved invaluable to the United States' World War II military forces. Aerial photographs were used to prepare aeronautical charts of inaccessible areas, to mark enemy positions and movements on maps, and to plan invasions. More domestic uses of aerial photography and photogrammetric products include investigations by oil, lumber, and power companies, highway and railroad commissions, inventorying, and forestry.

1.   Mechanics behind Photogrammetry

Stereoscopic vision allows an observer to see the height and depth of a photograph in addition to lengths and widths. The phenomenon of depth perception is possible due to the physical distance between the human eyes as this provides the brain with slightly different viewing angles of the same scene. An equivalent setup can be accomplished artificially by taking photographs of the same object or scene from different angles and viewing them side by side with a scanning stereoscope, as seen in Figure 9.

Figure 9.   Scanning Stereoscope (from "Old Delft," 2009)

A stereoscope allows an observer to look at the two overlapping photographs of a stereopair simultaneously but with each eye looking at one image instead of both eyes looking at the same image. To work correctly the photographs are taken in the same plane and lined up parallel to the ocular base of the instrument. For vertical aerial photographs the line of flight of the aircraft should be used to align the photographs on the instrument. When prepared correctly, the result is a miniature model seen in relief, called a

stereoscopic model or stereogram. Another technique for obtaining stereoscopic models includes printing two overlapping photographs in complementary colors on the same sheet. Special glasses are worn, with each lens being tinted the same color as one of the images, so that the observer sees one photograph with each eye. This creates a miniature relief model in black and white (Church, 1948).

For measuring distances in the models supplementary tools are needed. A measuring stereoscope includes a "floating mark" in each eye-piece to help define the line of sight and measure parallaxes. A stereocomparator additionally has a "system for reading the rectangular coordinates upon its photograph" (Church, 1948). In order to draw planimetric and topographic maps a multiplex projector is required. This instrument utilizes a collection of projectors to display adjacent photographs onto a plotting table, called a platen (Church, 1948). Two projectors are used at a time, one with a red lens and the other with a blue-green lens, and when their rays intersect the observer moves the platen around the model to mark different elevations on the map (Church, 1948).

2. Computer Photogrammetry and MVS

It had been hypothesized since the 1960s that computers could be used to analyze imagery. In 1969, Azriel Rosenfeld suggested methods for classifying entire images by the relationships among objects within them (Rosenfeld, 1969). Two years later, Lynn Quam reported on digital techniques for detecting change between images including those taken from different viewing angles (1971). As seen in Figure 10, simple change detection was completed by differencing two images, with areas of high dissimilarity indicating a change between the two. Papers such as these laid a foundation for future computer vision work and digital photogrammetry.

Figure 6-5a
7F78 Aligned

Figure 6-5b
7F77 Aligned

Figure 6-6a
7F78 - 7F77

Figure 6-6b
7F77 - 7F78
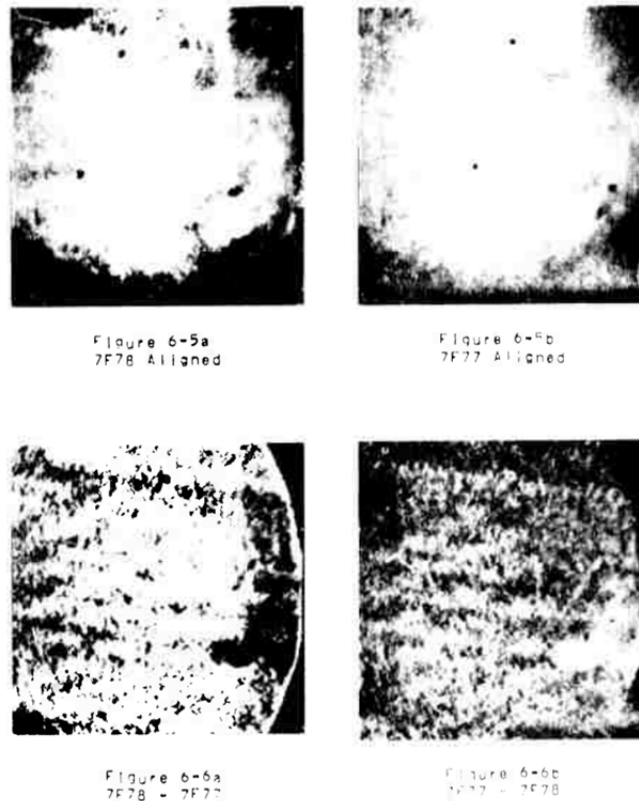
Figure 10.   Quam Differenced Two Images from the 1969 Mariner Mission to
Mars as a Form of Change Detection (from Quam, 1971, p. 77)

According to Dr. Joseph Mundy, the goal of digital photogrammetry is to "find the set of camera parameters, image feature positions and ground control point positions" that minimizes total error (1993). In manual photogrammetry exact camera parameters and positions are known because photogrammetrists strictly collect such information for mapmaking. Although time-consuming, it is fairly easy to match features in stereopairs because the two photographs are taken from similar angles.

Some computer software, such as BAE Systems' SoftCopy Exploitation Toolkit, (SOCET) follows strict photogrammetric rules. SOCET originated from fully digital analytical plotters, called photogrammetric workstations, created by photogrammetrist Uuno Vilho Helava in the 1970s (Walker, 2007). While these plotters have become more automatic over the years they still require a good deal of manual input. Large amounts of camera information are required to register images because SOCET relies on "faithful, mathematical sensor modeling" and image metadata to orient and triangulate imagery

(Walker, 2007). Possible SOCET inputs include camera model, interior and exterior orientation, calibration information, and GPS location, as well as tie points or ground controls points (GCPs). Products include 2-dimensional (2D) feature mapping around buildings, 3D point clouds either regularly gridded or in a Triangular Irregular Network (TIN), DEMs, DSMs, ortho-images, and mosaics.

In 2013, an initial comparison revealed that stereo point clouds created with SOCET using either aerial or satellite imagery accurately portrayed object locations but vegetation and building edges were less defined than LiDAR point clouds (Basgall, 2013). The difficulty with vertical walls around buildings was due to the method of point cloud creation. SOCET's stereo point cloud generator first created a DEM, which identified matching points between the images but continued by interpolating to create a 0.15m grid. This means that where cars, trees, or buildings were in close proximity the surface morphed them together in the DEM and the output point cloud. The result is not surprising because most photogrammetric outputs are actually 2.5-dimensional (2.5D) meaning they do not allow more than one point at any x,y location even with distinct z values. This makes representing truly vertical walls impossible, leaving them as unknowns in most models. Matching vegetation between images is also challenging because separate leaves and branches may move between collections or may be smaller than the image resolution. Even facing these difficulties Basgall's comparison revealed the SOCET output could still be used for change detection of sizable events (2013).

New software with roots in the computer vision community is trying to make image registration fully automatic. By teaching computers how to match features between images the human component is removed. A survey by professors at the University of Washington concluded there are four main categories of multiview stereo (MVS) algorithms (Seitz, 2006). The first of these compute a cost function to determine which surfaces to extract from a 3D volume. Seitz and Dyer proposed a method for coloring voxels by finding locations that stay constant throughout a set of images (1999). A second class includes space carving techniques such as those based on voxels, level sets, or surface meshes that progressively remove parts of a volume according to the imagery (Seitz, 2006). One of these methods, described by Eisert, Steinbach, and Girod,

15

uses two steps to first, assign color hypotheses to every voxel according to the incorporated images and second, either assign a consistent color or remove the voxel (1999). Algorithms in the third class compute depth maps for input images and merge them together to create coherent surfaces (Gargallo & Sturm, 2005). The last class includes methods which extract and match features between images before fitting a surface to the registered points. Morris and Kanade suggested starting with a rough triangulation of a surface and refining it to better represent the objects found within the input images (2000).

Due to the vast number of pixels found in a single image and the amount of time it takes to compare all of them, older algorithms were taught to identify a handful of unique features and compare those to the unique features found in other images. Now that computer hardware has progressed, lifting previous time constraints, dense pixel-wise matching algorithms are available that can search every pixel or window of pixels for a match (Hirschmuller, 2005). The large numbers of matches found in this way allow for the creation of very detailed 3D models. Heiko Hirshmuller's semi-global matching (SGM) algorithm maintains sharper object boundaries than local methods and implements mutual information (MI) based matching instead of intensity based matching because it "is robust against many complex intensity transformations and even reflections" (2005). SGM's pathwise aggregation uses cost information from eight directions to minimize disparity, with its major attraction being that its runtime is linear to the number of pixels and disparities (Hirshmuller, 2011).

Developments in the computer vision community over the last 10 years have also led to the creation of algorithms that can determine camera orientation automatically. Software such as Bundler, Microsoft Photosynth, Agisoft PhotoScan and PhotoModeler solve for camera parameters and generate 3D point clouds of either objects or scenes (Harwin, 2012). Some can reconstruct objects and buildings from unorganized collections of photographs taken from different cameras at multiple distances, viewing angles, and levels of illumination (Agarwal, 2011). Matching features in such dissimilar images requires identifying interest points within each photograph, with the more rigorous algorithms finding affine-, in-plane rotation-, translation-, and illumination-invariant

features (Van Gool, 2002). The scale invariant feature transform (SIFT) operator has proven especially robust and has grown in use since 2004 (Lindeberg, 2012).

Structure from motion (SfM) is another technology that utilizes multiview techniques. It falls between photogrammetry and MVS by using overlapping photographs taken by a single camera around an object. The motion of the camera between semi-stereopairs is used to determine position and orientation so the correct geometry can be applied to build 3D models. See Figure 11 for an illustration of the relationships between the three techniques mentioned.
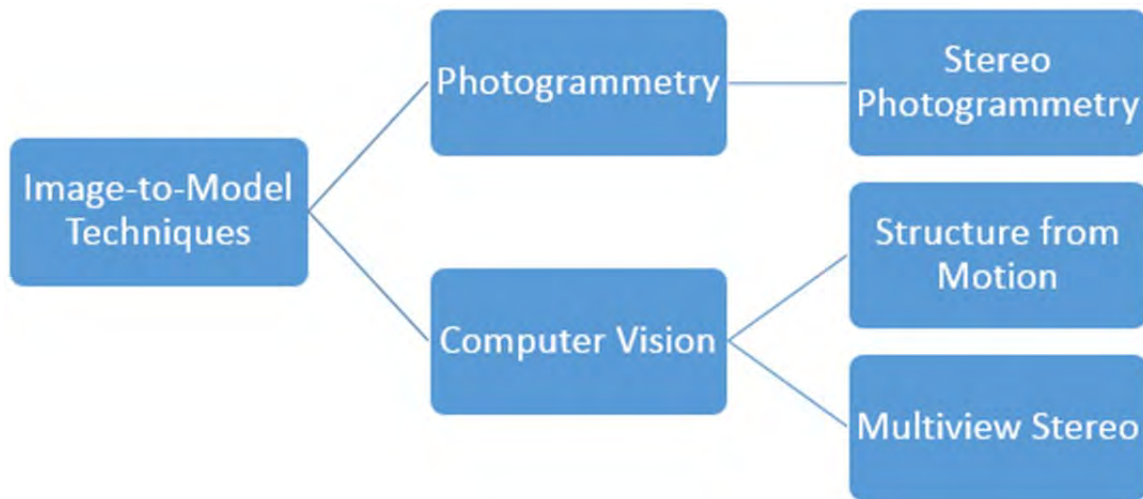
Figure 11.   Block Diagram Illustrating Relationships between
Image-to-Model Techniques

3.   How It Works

Triangulation is the basic mathematical concept behind photogrammetry. Stereo vision exploits the slightly different views between two photographs to derive depth and create 3D models. As seen in Figure 12, it is necessary to know the two camera locations (C1 and C2) in order to correctly locate the objects (P and Q) in 3D space according to their images (P'1, P'2, Q'1, and Q'2). Accurate image correspondences are required for 3D reconstruction so coordinates can be derived from intersecting optical rays (Faugeras & Keriven, 2002). By finding the intersection of the lines extending from each camera through its respective image, the depth of each object can be determined.
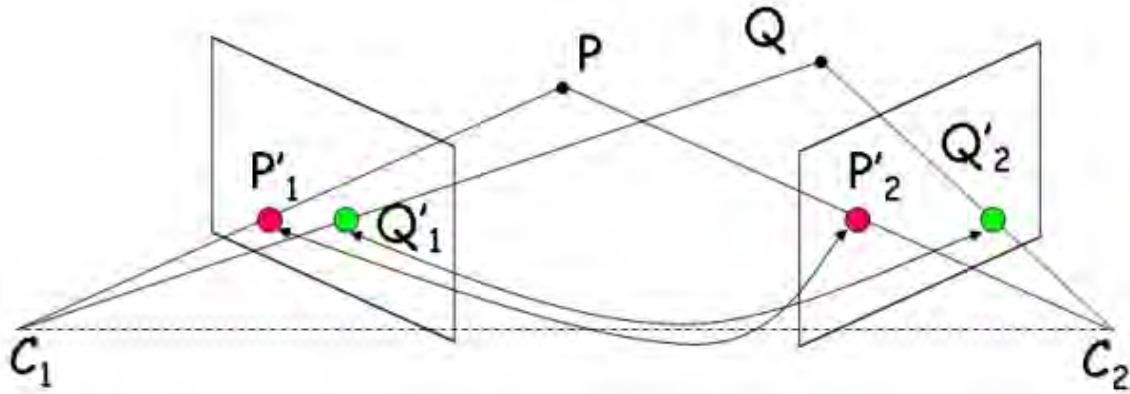
Figure 12.   Deriving Depths of Points P and Q using Two Images
(from "Image-based Measurements," 2008)

If the camera's position and aiming angle are unknown, resection is required to determine the missing information. Resection uses a given image to determine three position coordinates and three angles in order to correctly derive the location of the camera and the angle it was pointing at the time the photograph was taken. Resection, if done manually, is a long tedious process, which is why the automatic computer vision approach is highly desirable. Cameras must also be calibrated before use so that detected errors can be removed before imagery is processed. Altogether these techniques (triangulation, resection, calibration) are referred to as the bundle adjustment. In some computer vision algorithms triangulation and resection are computed at the same time, minimizing errors in each until an optimal solution is found.

Once feature coordinates are determined, points are created in 3D space. Photogrammetric point clouds are limited to the area of overlap between the two included images and can only contain one height coordinate for each latitude and longitude, similar to LiDAR point clouds. MVS point clouds are not quite as limited, revealing walls and other vertical structures provided they were visible in multiple images and correctly matched.

18

B.   LIDAR BACKGROUND

While most people are familiar with radar and its ability to determine the location of objects by using radio waves, light detection and ranging (LiDAR) has gained popularity within the last 30 years. LiDAR is a technology that utilizes many radar principles, but applies them to shorter wavelengths: in the visible to infrared range.

Surveyors used the first terrestrial laser instruments to replace tungsten and mercury vapor lamps in the 1970s. Newly invented lasers allowed a small team to measure long distances and apply trilateration techniques in order to create topographic maps quickly and efficiently (Shan & Toth, 2009). Current electronic total stations (ETSs) measure angles and distances from their location to that of their corresponding prism reflector using modulated infrared signals. Figure 13 shows how ETSs can determine vertical height measurements that are out of reach of ground-based prisms.
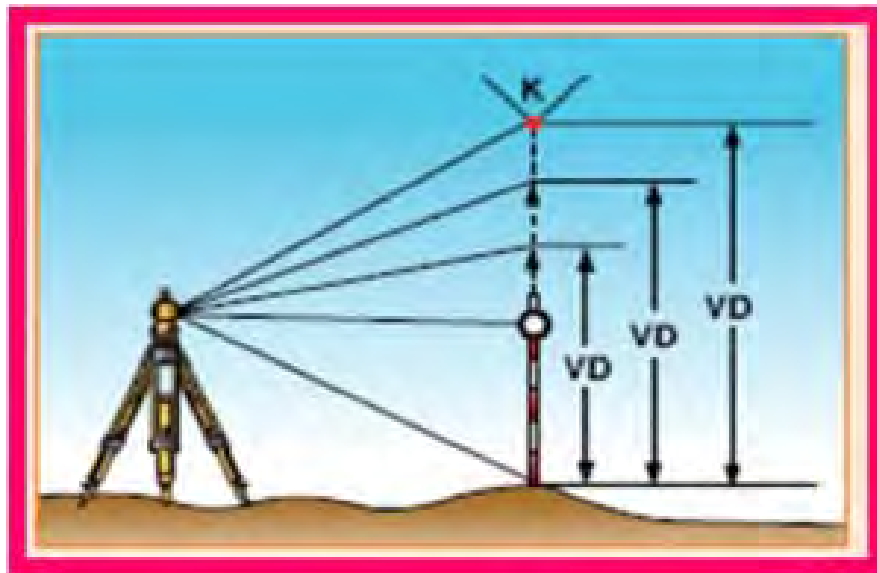

Figure 13.   Electronic Total Stations Measure Heights of Unreachable Objects
                Via Remote Elevation Measurement (from "Total Station," n.d.)

By timing how long it takes the infrared signal to travel to and from the prism, very accurate distances can be determined. This idea, when carried out in a scanning mode, allows one unit to measure distances to multiple objects, returning large numbers of points that can be converted into 3D space and used to build 3D models. Terrestrial LiDAR has been found useful in a multitude of applications such as "bridge and dam monitoring, architectural restoration, facilities inventory, crime and accident scene analysis, landslide and erosion mapping, and manufacturing" (Schuckman, 2014).

LiDAR has also been adapted to collect from airborne platforms. When carried on the underside of an airplane or unmanned aerial vehicle (UAV) large swaths of land can be covered in a few hours. Airborne sensors usually operate in a whiskbroom mode, sweeping a laser in a "sawtooth" pattern of points, back and forth across the flight path. This mode takes advantage of the forward motion of the aircraft to cover the ground below (Diaz, 2011). The speed of the aircraft and the pulse rate of the sensor determine the resolution, or point density, of the point cloud that can be created. Airborne systems are able to concentrate on moderately sized areas such as cities, coastlines, and national parks. Multiple flight lines are collected, usually in parallel, with enough overlap so each strip can be stitched to adjacent ones and a continuous surface model can be created.

1.   Physics of LiDAR Systems

Modern LiDAR units consist of three integral components, seen in Figure 14, to ensure accuracy and usability of the collected data. The laser rangefinder is arguably the most important apparatus, as it actively emits and then collects laser energy like the terrestial ETSs, but for airborne systems the Global Positioning System (GPS) and the inertial measurements unit (IMU) are required if the collected data is to be geolocated and correctly fused.
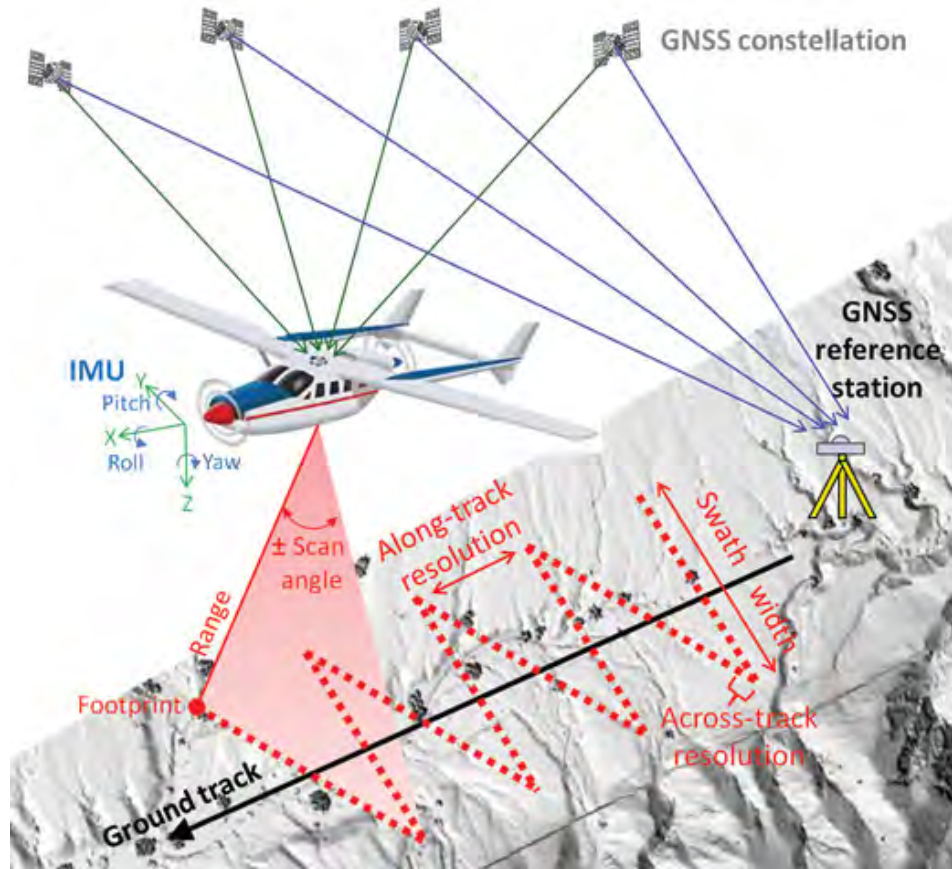
Figure 14.   Main Components of Airborne LiDAR (from Diaz, 2011)

The main laser unit employs a laser which emits pulses of photons. When these pulses travel to the ground, reflect off objects and the earth's surface, and return to the aircraft the photodetector collects and records their intensity level and time of return. Most systems use the time of flight (TOF) method to determine the range of the objects illuminated by the laser. The TOF method determines the distance between the aircraft and the illuminated object, providing the height information for post-processed points in the 3D model. Due to atmospheric effects, mechanical issues, and human error it is impossible for an aircraft to stay perfectly straight and level during a survey so an IMU is also required. IMUs take these factors into account and precisely track the attitude of the aircraft, recording changes in the roll, pitch, and yaw at all times during a collection so that these measurements can be processed with the data.

GPS systems provide position and velocity information so that points within the data set can be referenced to real points on the surface of the earth. Due to factors such as the wavelength of light produced by the laser source, the pulse repetition frequency (PRF), and the speed of the aircraft, the entire surface of the ground will not be mapped. Instead, points will be collected at intervals along the laser's path. The point density, usually measured per square meter, indicates the resolution of objects that can be seen in a particular scan.

Once all points are collected, flight paths are stitched together and software is used to visualize the 3D point cloud. The GPS provides the x and y coordinates, latitude and longitude, while the determined range indicates the z, or altitude coordinate. Certain software can now identify points within a point cloud according to height and separate them into categories such as ground, buildings, and trees. If color imagery is collected of the same area on the ground, software can overlay this data onto the point cloud to produce true-color 3D scenes. The best results occur when the LiDAR scan and imagery are taken simultaneously so that objects prone to movement, such as cars, people, and water, appear in the exact same location in both datasets.

III. DATA AND SOFTWARE

A. LIDAR AND IMAGERY OF NPS

LiDAR data were collected in October of 2012 by Watershed Sciences, Inc. (WSI). It utilized an Optech Orion C200 laser system flown on a Bell 206 LongRanger helicopter. A good portion of the Monterey Peninsula was collected; Figure 15 shows the extent of the area around the Naval Postgraduate School (NPS) to be studied here. As the LiDAR data were saved in tiles less than 200 Megabytes, 12 such tiles were required to represent the entire NPS campus.

Figure 15.   LiDAR Dataset of the NPS Campus East of the Monterey Peninsula (map from Google Maps, n.d.)

Even flying at 450m altitude the LiDAR point cloud was very dense at approximately 30 points/m^2, allowing for sub-meter objects to be identified. The point cloud seen below includes RGB coloring from photographs taken of the same area. This extra encoding aids in the identification of different surfaces. Figure 16 demonstrates how the vertical surfaces of buildings, such as the front façade of Hermann Hall, are missing due to the vertical nature of LiDAR collection. However, details such as roof shape, tree leaves, cars in the parking lot, and even the flagpole are present. Compare the structures shown in the LiDAR dataset to a photograph taken of Hermann Hall and the surrounding buildings.
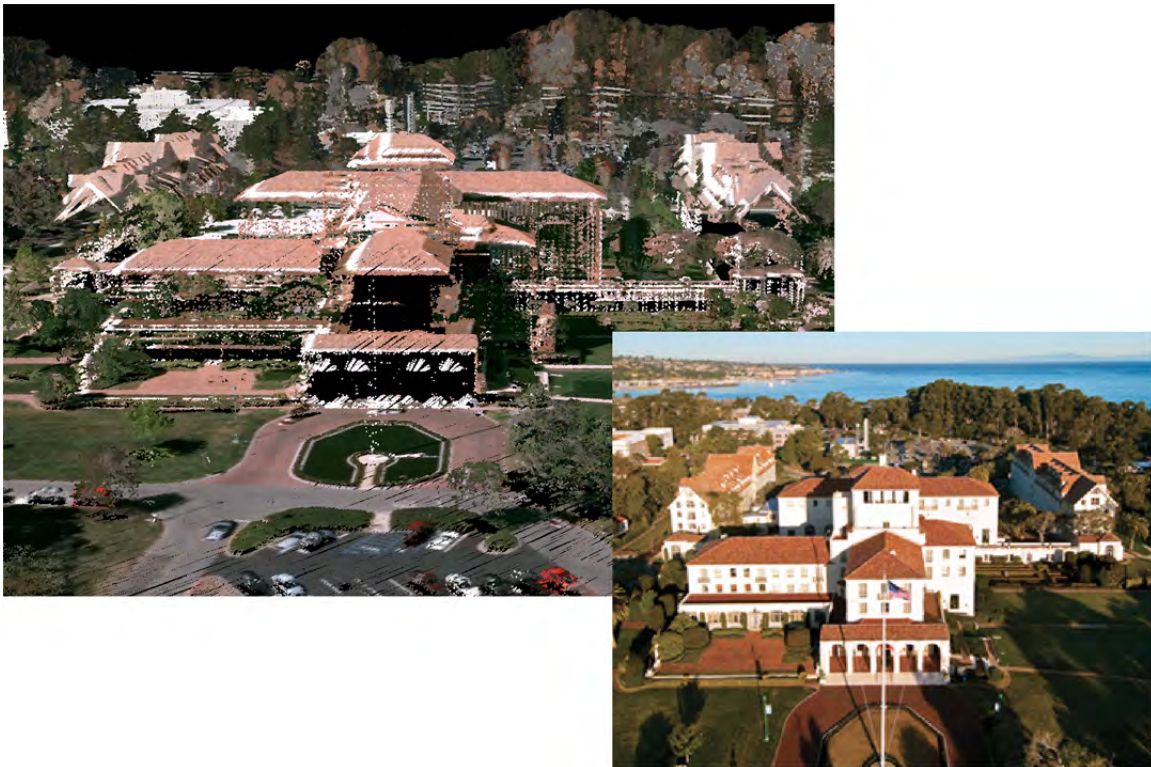
Figure 16.   LiDAR Dataset Compared to a Photograph of Hermann Hall
(from "NPS Statistics," 2014)

B.   AIRBORNE DATA

Optical imagery was obtained in both October 2013 and May 2014 using a Hasselblad H4D-50 50 megapixel camera. This imagery was likely taken from a small airplane similar to a Partenavia SPA P68C from an altitude of 433m which produced 5cm pixel resolution (University of Texas, 2013). In both the October and May collects six of the images contained Glasgow Hall. Figure 17 illustrates the quality of the 2013 Hasselblad imagery used for this study.

Figure 17.   Close-up Near-nadir View of Glasgow Hall Aerial Imagery

Table 1 shows the similarity between the May and October collects. The two sequences were photographed from near-identical flight paths so the pairs are very similar. The top row exhibits the October 2013 images, taken during Monterey's sunny Indian summer, while the bottom row was taken in May 2014 on a cloudy day, useful because of the lack of shadows. They have been arranged so that the building's south side can be viewed in a west-to-east direction in the first three images, followed by three near-nadir views.

Table 1. Comparison of October 2013 and May 2014 Hasselblad
Imagery (Oriented Roughly North-South)

Aerial imagery was also collected by Watershed Sciences, Inc (WSI) in October 2012. This collection was flown at 450m yielding a pixel resolution of 10-15cm with an UltraCam Eagle camera produced by Microsoft. Again, six of the images contain Glasgow Hall, and due to very oblique angles in three of the images the rear of the building is visible. In Table 2, the first three images show the south side of Glasgow on a west-to-east flight path and the last three images similarly show the north side.

Table 2. UltraCam Eagle Imagery of Glasgow Hall

C.   SATELLITE DATA

A small collection of satellite imagery covering the Monterey, CA area over the years 2000 to 2011 was accessed, providing seven usable images of NPS. Table 3 exhibits each image and provides the panchromatic resolution given on the Digital Globe website for each of the mentioned satellites.

#	Year	Month	Day	Satellite	Panchromatic Resolution	
1	2000	Nov	28	IKONOS	82 cm	32 in
2	2000	Nov	28	IKONOS	82 cm	32 in
3	2002	Sep	21	Quickbird I	61 cm	24 in
4	2002	Oct	29	IKONOS	82 cm	32 in
5	2008	Dec	26	Worldview	46 cm	18 in
6	2009	Oct	28	Worldview	46 cm	18 in
7	2011	Jan	19	GeoEye 1	46 cm	18 in

Table 3.   Satellite Imagery Thumbnails, Date of Collection, Run Number, and Details (after Digital Globe, 2013)

27

The IKONOS satellite is the oldest one of the group, having been in orbit since 1999. Following the launch of IKONOS were those of Quickbird I in 2001, Worldview-1 in 2007, and GeoEye-1 (previously Orbview 5) in 2008 (Digital Globe, 2013).

D.   SOFTWARE

The IMAGINE Photogrammetry software application, formerly Leica Photogrammetry Suite, extracts information from stereopairs to create 3D models. In the works since 2003, it now contains three methods for producing terrain models. The automatic terrain extraction (ATE) process creates medium density DTMs rapidly and requires little manual editing. The enhanced ATE (eATE) process generates higher resolution models using stereopairs and can also take advantage of parallel processing to decrease runtime. The 2014 release of IMAGINE Photogrammetry unveiled a SGM algorithm that can create models with point spacing to rival that of LiDAR. SGM is currently only applicable to aerial imagery but Intergraph is looking to update the algorithm for its 2015 release. For this thesis the eATE module was applied to both aerial imagery, in TIF, and satellite imagery, in NTF.

For MVS purposes, Agisoft Photoscan Professional, from here on referred to as Agisoft, offered itself as a suitable software package. Agisoft allows any user to upload a variety of photos and generate 3D models. The software is sensor ambiguous as it completes a bundle adjustment for each image without supplementary information, determining camera angle and location before building 3D models automatically. While created to work with aerial imagery, Agisoft was able to ingest satellite photos once they'd been converted to TIFF. The product website also indicates it can accept inputs of JPEG, PNG, and BMP.

Quick Terrain Modeler (QTM) and CloudCompare (CC) are visualization packages designed to display 3D point clouds. They both have the capacity to express multiple models simultaneously making side-by-side comparison possible.

28

IV. PROCESSING, RESULTS, AND ANALYSIS

A. AERIAL IMAGERY MULTIVIEW STEREO

Having access to three aerial imagery datasets allowed for a number of combinations to be tested. The Agisoft website and those of similar software packages lead a user to believe that the more images included in the process the more complete the model turns out. It was found this was not necessarily the case, as explained in the three trials below.

The two Hasselblad datasets were collected using similar flight paths so the images provided only slightly different views of Glasgow Hall, while the WSI dataset included very oblique angles and provided much better views of the sides of the building. Trial #1 used equal numbers of images from each dataset, working from one to six so that the first trial was composed of three images and the last trial contained all 18. In Trial #2 the best model created in Trial #1 was compared to dense models created with the six images in each separate dataset. Finally, Trial #3 dissected the winning model from Trial #2 to see if all six images were really necessary or whether a model created using three, four, or five photographs was sufficient, or even superior in completeness.

1. Trial #1

Images in this trial were added in such a way as to provide the most new information in the first three runs before adding the repeat images from the Hasselblad datasets. Because the WSI imagery covered a much larger area, each image had to be subset within Agisoft to focus on the Glasgow Hall area. Subsets included Glasgow Hall, the Dudley Knox Library, and surrounding parking lots in order to cover the same subject matter as the Hasselblad imagery, as seen in Figure 18. This was the extent of pre-processing required by the Agisoft software.
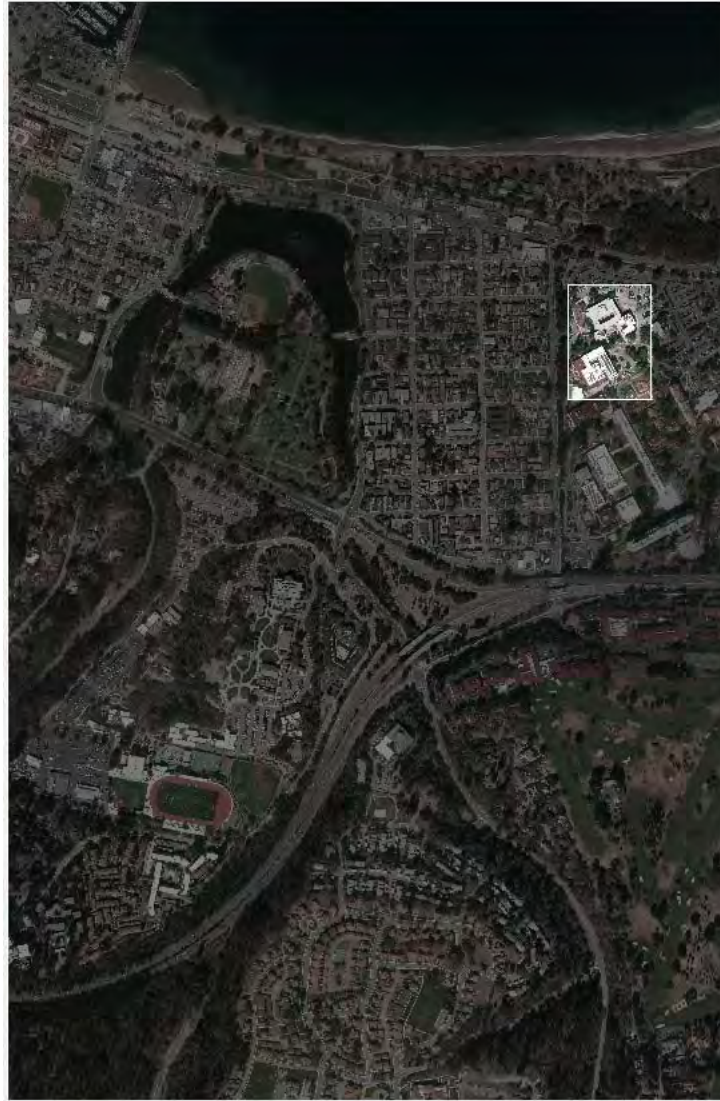
Figure 18.   WSI Image Subset to Glasgow Hall and Dudley Knox Library

After adding the preferred images (Workflow > Add Photos… > select from library) a sparse point cloud preceded any advanced models. The sparse cloud was created by aligning the photos (Workflow > Align Photos…), which is when Agisoft performs a bundle adjustment on each image to determine its location and pointing angle. The sparse point cloud is only a rough sketch, as seen in Figure 19. Each blue rectangle represents a camera's suggested position and the black line stemming toward the image name provides the suggested angle. In the lower left corner of the main window, the sparse point cloud is seen as white and gray points.
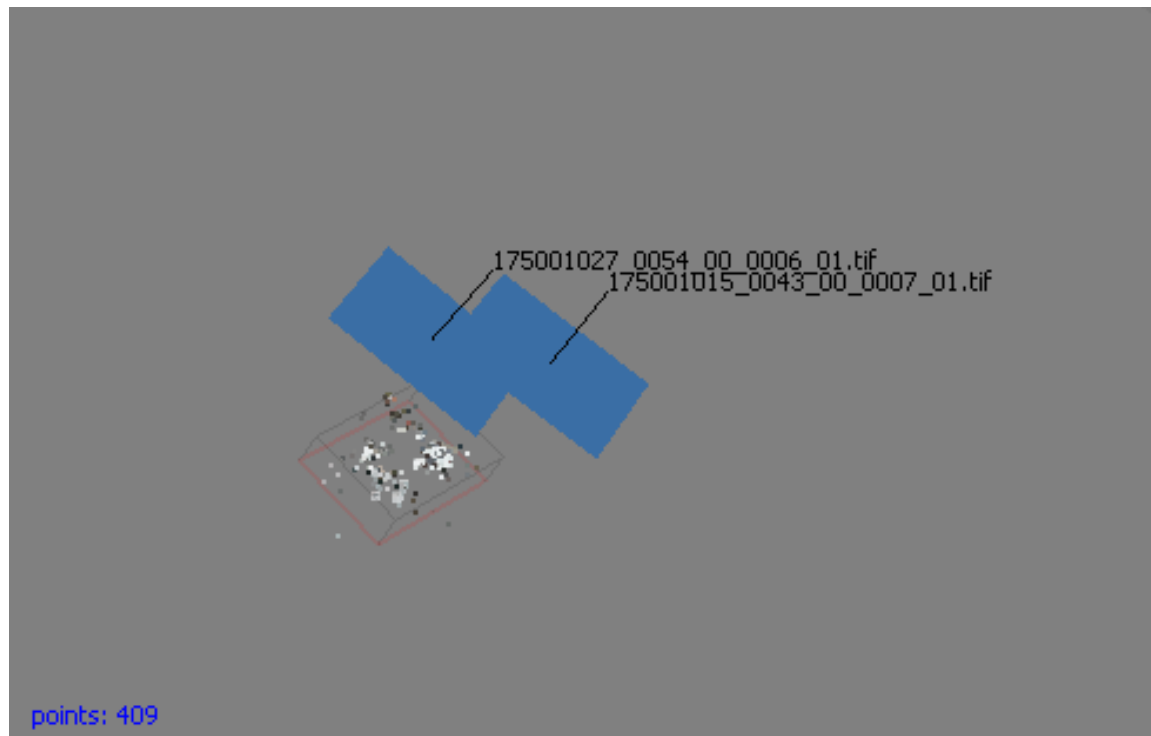
Figure 19.   Three Aligned Photos (One Off-screen) and Sparse Point Cloud

After the sparse point cloud laid the groundwork, the now-registered images were re-evaluated for matching features and a dense point cloud was created. As seen in Figure 20, dense clouds reveal structures and textures, especially when color imagery is available. The incompleteness of this dense point cloud was due to the lack of information, as only three images were run in this trial.
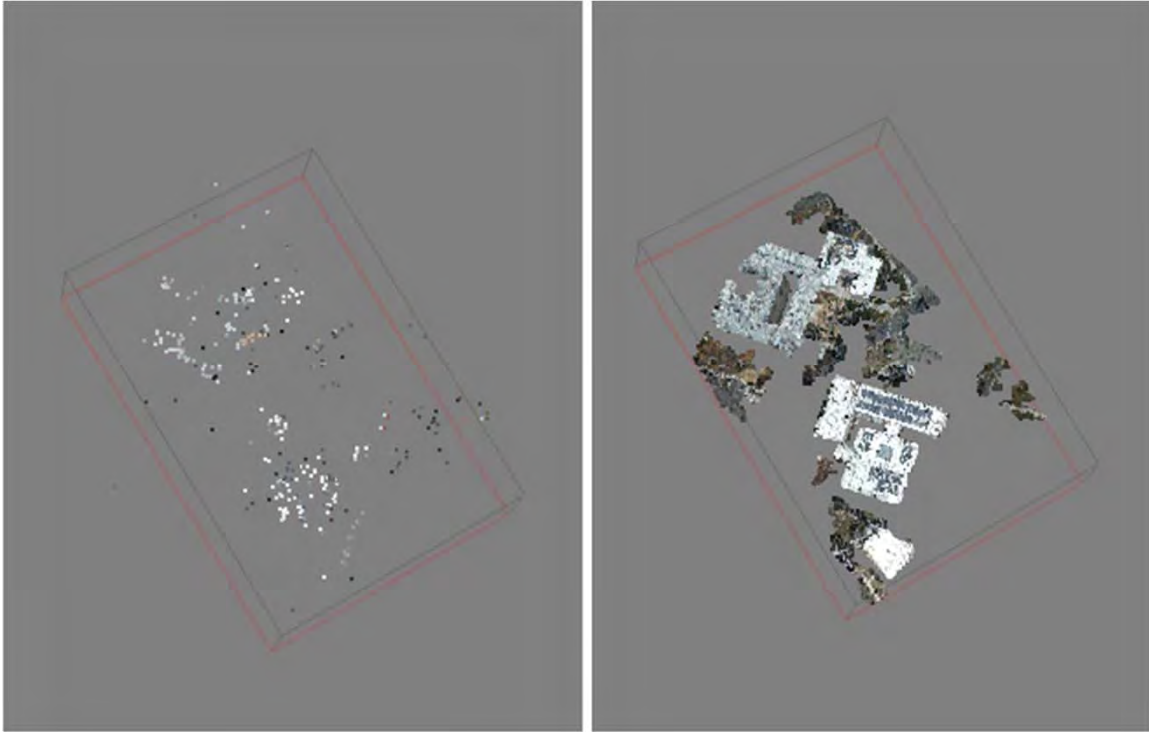
Figure 20.   Sparse and Dense Aerial Point Clouds in Agisoft

In Table 4, the progression of dense point clouds appears to reveal improvements from the first to the fourth runs. While the fifth and sixth runs begin to display pieces of Glasgow's southern wall they also appear fuzzy and speckled. The shape of Glasgow's roof is hardly discernable in the last run, indicating that adding more images degraded the model. For this trial Run #4 claims the title for best model.

Run #1: 3 Images

Run #2: 6 Images

Run #3: 9 Images

Run #4: 12 Images

Run #5: 15 Images

Run #6: 18 Images
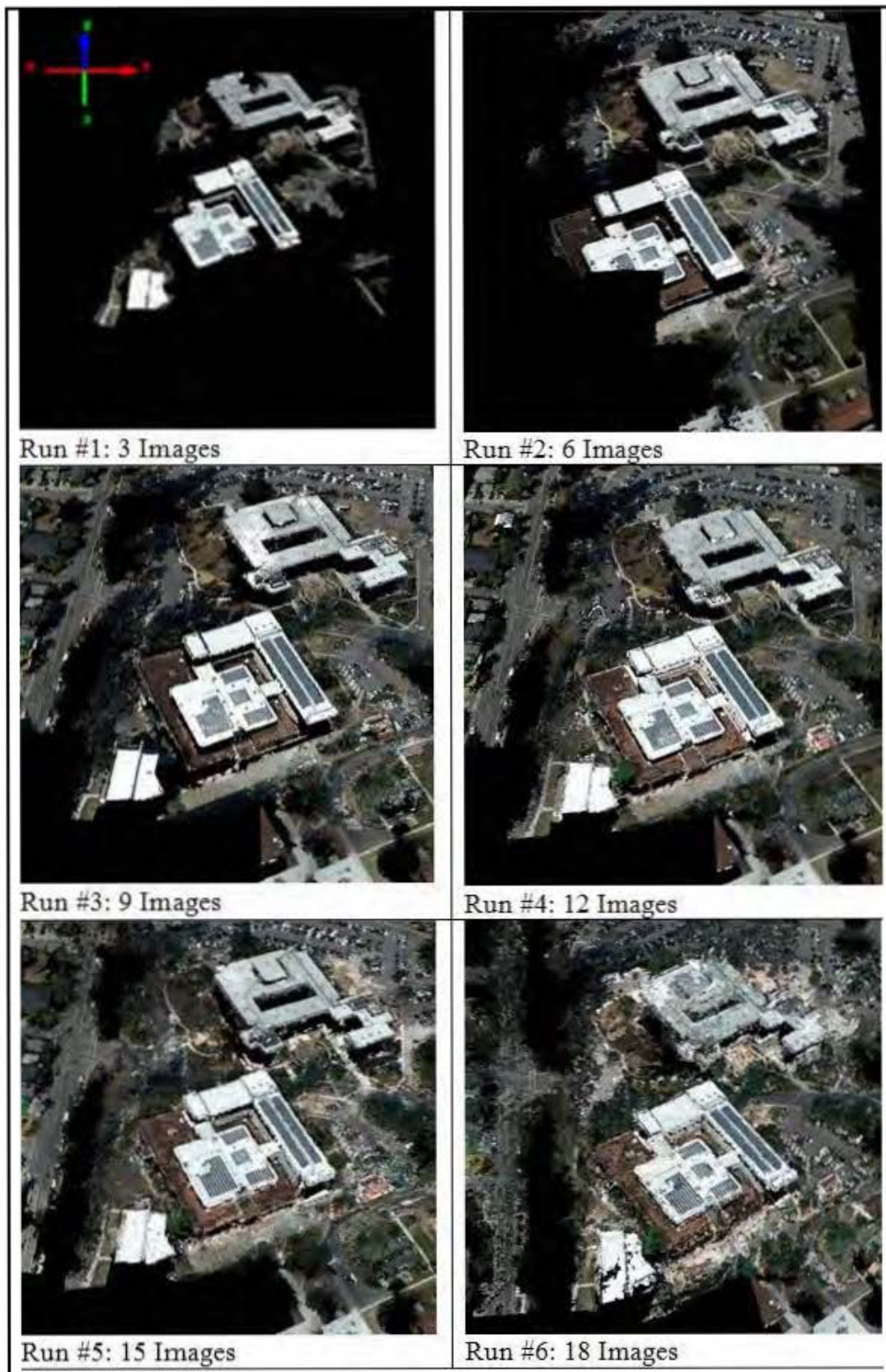
Table 4.   Dense Points Clouds for Trials Utilizing All Three Datasets

2. Trial #2

The goal of Trial #2 was to determine whether a single dataset could compete with the results of the combined dataset. Using Run #4 as the winner of Trial #1, the steps already mentioned were repeated for each of the image collections separately. Table 5 shows the WSI model a clear winner, as it contains the fewest holes, the most vegetation, and even walls of buildings.
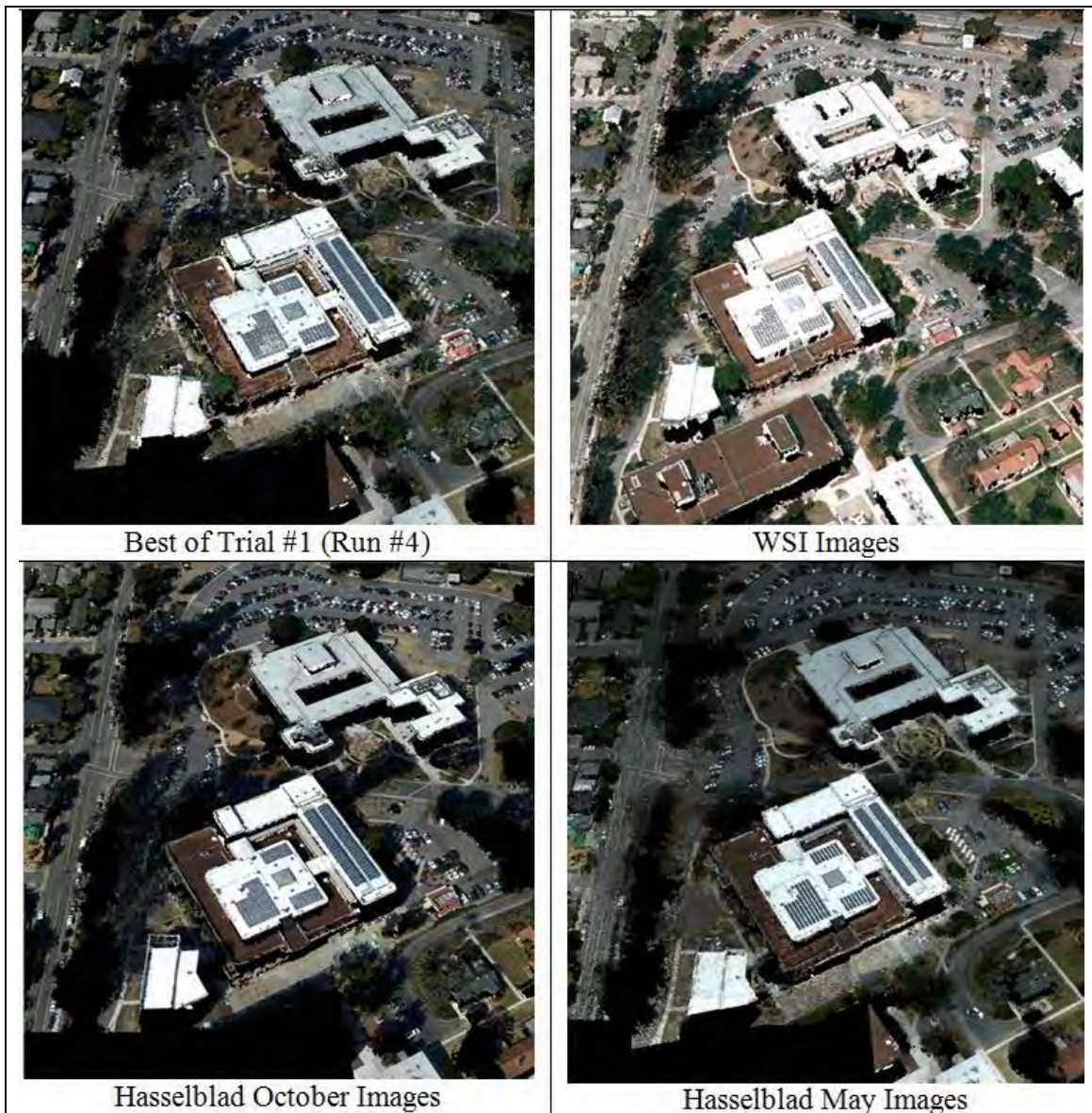
Table 5.   Models of Each Six-Image Collection Compared to Winning Combined Model, Using Aerial Imagery

3. Trial #3

For the final trial, the winning WSI model from Trial #2 was further evaluated. The first run started with three WSI images, chosen so that the largest differences in camera angle might provide the most information, with the last run containing all six images. Table 6 demonstrates changes between the models.

Run #1: 3 WSI Images	Run #2: 4 WSI Images
Run #3: 5 WSI Images	Winner of Trial #2: 6 WSI Images

Table 6.   Comparison of WSI Models

The winning model is not the expected run containing all six images. Comparing Run #3 and Run #4, small differences indicate a greater level of completeness in the model of only five images. Starting with the buildings it should be noted that the walls of Glasgow's highest protrusion, a white square-shaped room, are more complete in Run #3. Similarly, Glasgow's southernmost wall has fewer and smaller holes. This trend extends to the walls of the library and other nearby buildings. Due to the small number of images incorporated into these models the results seen above are surprising.

To further investigate the puzzling findings above another run was completed, switching the fifth and sixth images. In Run #3 of the last trial the fifth image was taken from a north-facing position while the sixth image was taken from a south-facing position. As seen in Table 7, by focusing on only the south walls of the buildings in Trial #3 half of the information was missed. In Table 7 it becomes clear the fifth images provided the information allowing Agisoft to model the building walls: the original five covering the southern walls and the new five covering the northern walls. After considering all views of Glasgow, the run containing all six images reclaims the title of best model, as it represents building walls on all sides, albeit incompletely.

This trial revealed that the order in which the images were added to the model changed the points registered with each iteration. If all images are eventually going to be included this does not affect the final outcome but for situations in which the number of images is limited care should be taken to include those containing the most unique information.

Original 5 WSI Images: South Side | Original 5 WSI Images: North Side

WSI with New Fifth Image: South Side | WSI with New Fifth Image: North Side

WSI Model with All 6 Images: South Side | WSI Model with All 6 Images: North Side

Table 7.   WSI Models of Five and Six Images

B.   SATELLITE IMAGERY MULTIVIEW STEREO

As Agisoft could not ingest the satellite images provided in National Imagery Transmission Format (NITF) they were converted to Tagged Image File Format (TIF). Then each image histogram was stretched to cover the full bit range to create the greatest contrast between shades of gray. AgiSoft was run with each set of images; first by aligning them and creating a sparse point cloud, and then creating a dense point cloud after the model passed initial inspection. Table 8 shows the progression of images run through the software. The first three include one of each resolution, followed by the IKONOS images at the lowest resolution of 82 cm, and finally by the higher resolution images at 46 cm.

Image #	Run #	Year	Month	Day	Satellite	Panchromatic Resolution	
1	1	2000	Nov	28	IKONOS	82 cm	32 in
3	1	2002	Sep	21	Quickbird II	61 cm	24 in
6	1	2009	Oct	28	Worldview 1	46 cm	18 in
4	2	2002	Oct	29	IKONOS	82 cm	32 in
2	3	2000	Nov	28	IKONOS	82 cm	32 in
5	4	2008	Dec	26	Worldview 1	46 cm	18 in
7	5	2011	Jan	19	GeoEye 1	46 cm	18 in

Table 8.   Order Satellite Images were added to Agisoft Photoscan Pro

After completing each run the dense point cloud was exported in .las format and viewed in QTModeler software for comparison. As seen in Table 9, with each image addition more of the Monterey Peninsula became visible. By returning to Table 3 the reader can see that while the three original satellite images cover much of the same area only a thin strip of the peninsula was correctly registered. Another oddity is found in the run of five images where the northeastern tip of the peninsula is missing when it was clearly present in the run before, a run containing four of the same images.
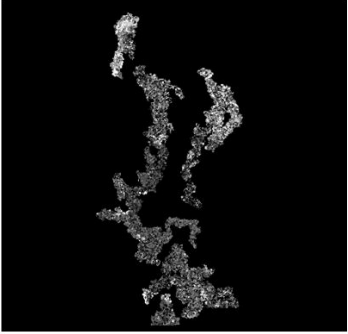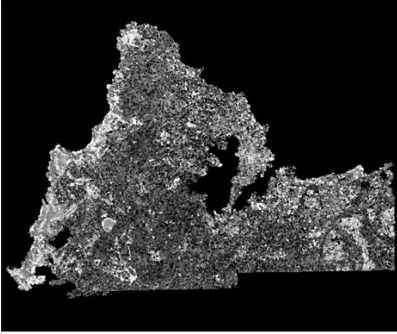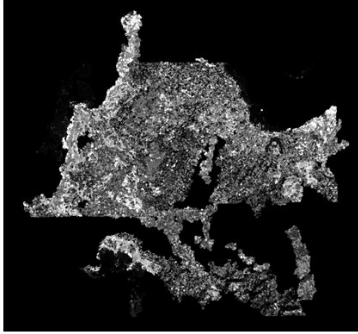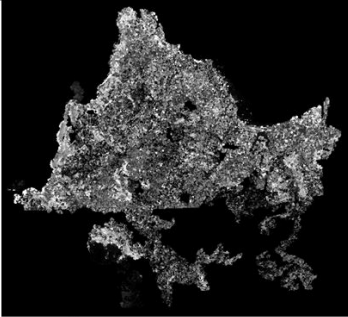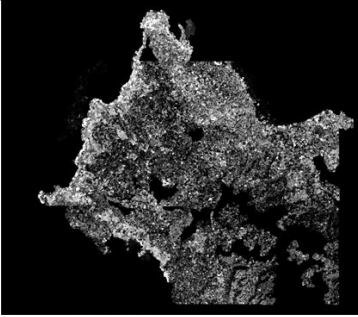
| Run #1: 3 Images | Run #2: 4 Images | Run #3: 5 Images |
| Run #4: 6 Images | Run #5: 7 Images | |

Table 9.   Five Successive MVS Runs, Adding One New Satellite
Image Each Time

According to Table 9, it would appear that the final run is the most complete. This suggests that more images would continue to improve the model and that up to this point there is not an ideal number of images to include. Further work to find the ideal number may be completed in the future.

By taking a closer look at the NPS campus, we hope to determine the usability of each model. As seen in Table 10, we find that the more images included the better the model. An image for the first run was not included because it did not discernably contain the NPS campus. We ignore Del Monte Lake in the top right corner because water's ever changing surface disallows point registration. The second run of four images may seem to be full of shadows but these black areas actually indicate unregistered surfaces. Most are seen around trees and buildings, although in the second run there are many spots remaining in open areas which were well imaged. The third run has an even less complete model, with parts of the campus completely missing, especially in vegetated areas. The fourth and fifth runs are fairly complete, with the fourth showing a few rough spots

around forested areas and the fifth missing part of a baseball diamond and parking lot, as well as some of the academic buildings on the west end of campus.
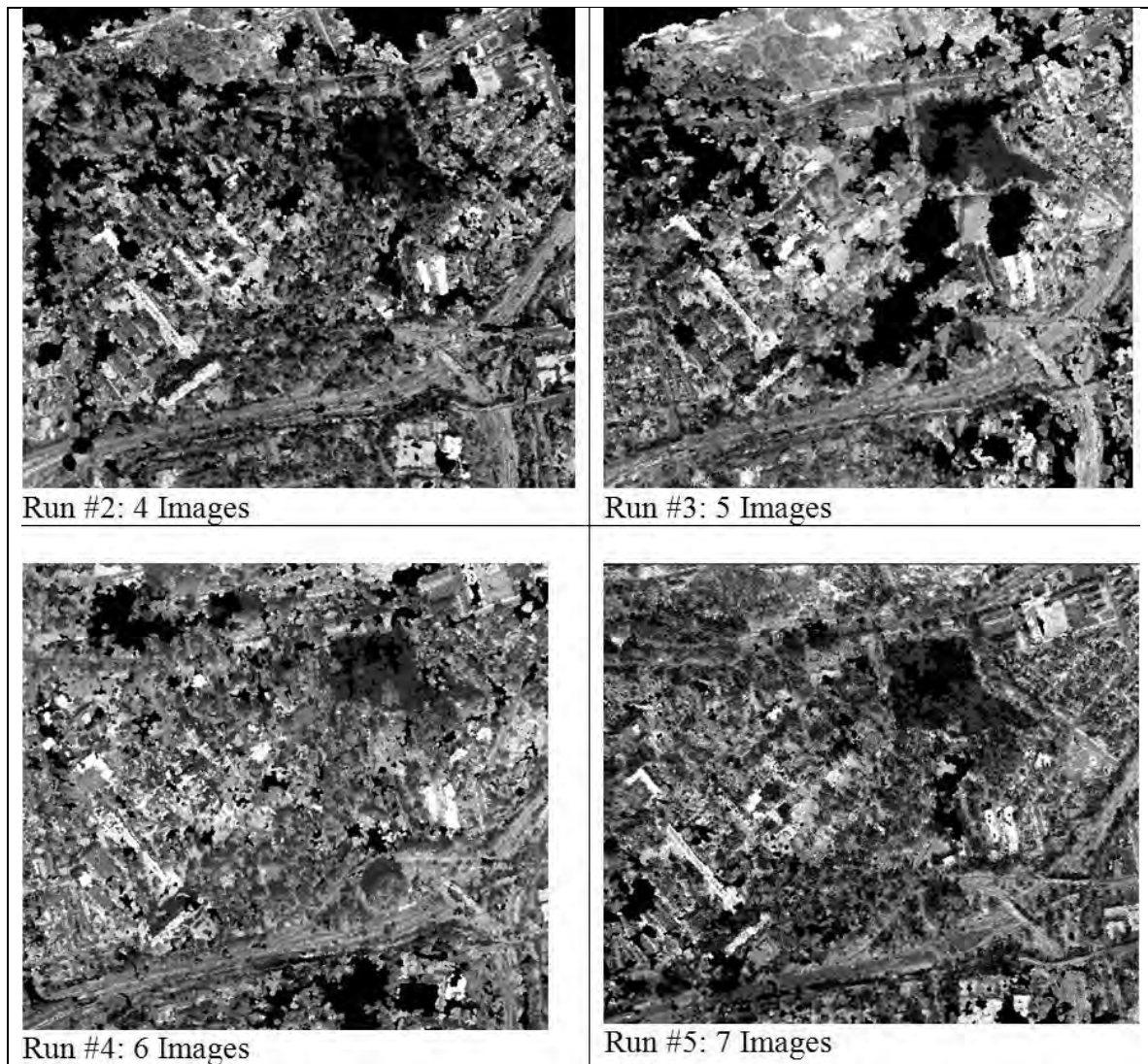

Table 10. Satellite MVS Close-up of NPS

If we were only interested in the nadir view of each model we could simply compare each one to a map of the area. When considering 3D models we must also evaluate the altitude or elevation component, the third element of xyz models. The second run appears to have points on at least four different planes, while the third, fourth, and fifth runs appear to contain five, four, and two planes, respectively. It appears the

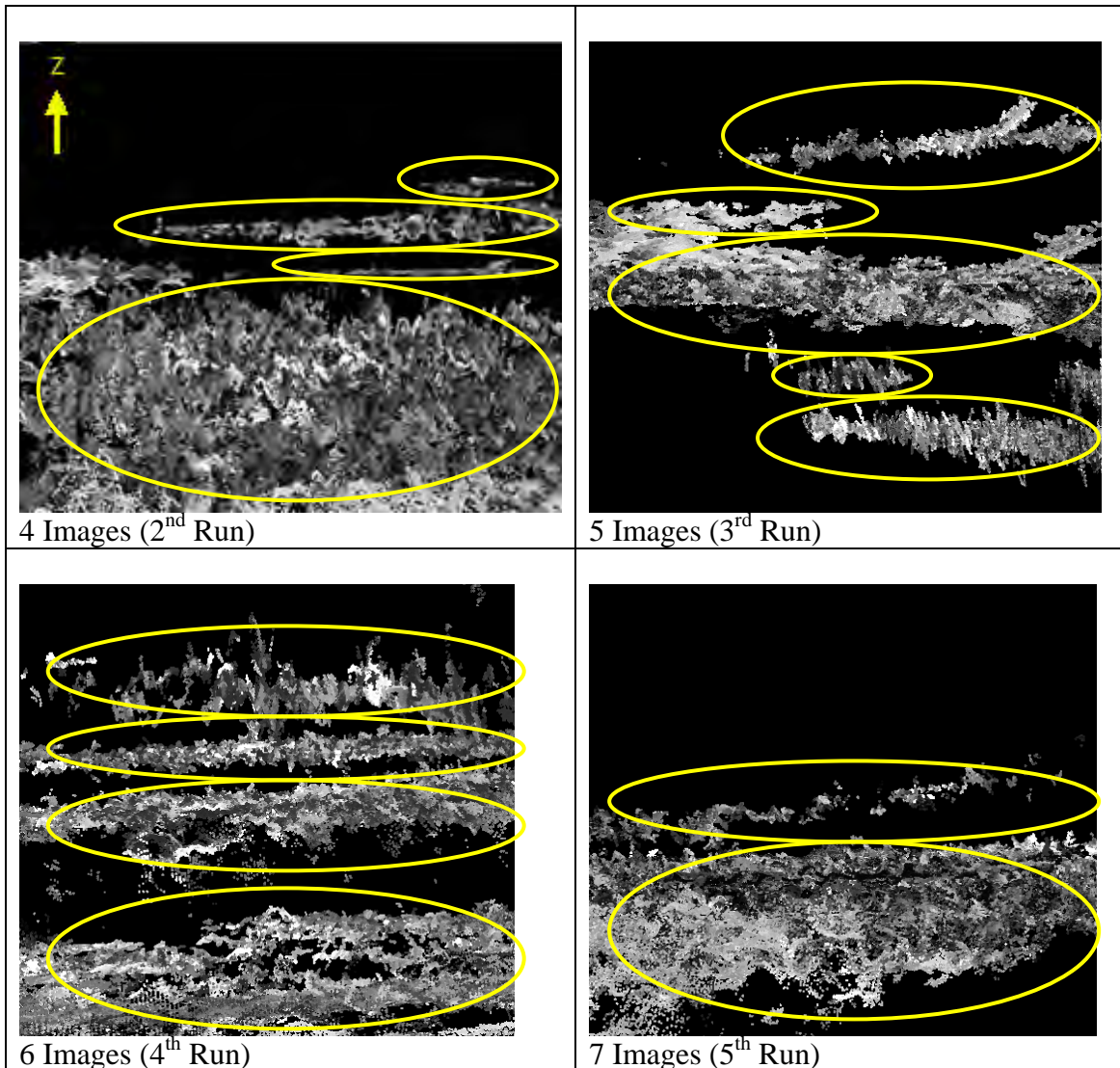Agisoft software, which assumes a framing camera system, is unable to vertically rectify satellite imagery.

4 Images (2nd Run)	5 Images (3rd Run)
6 Images (4th Run)	7 Images (5th Run)

Table 11. Side-view of Satellite MVS Models, Indicating Z-Errors

C.   PHOTOGRAMMETRIC MODELS

The IMAGINE Photogrammetry module is designed to work with data obtained from commercial aerial and satellite systems. Upon opening, a new Block file must be created to hold detailed inputs. The camera model must be specified, whether it be a frame, digital, or video camera, a pushbroom sensor, or a satellite. Projection

information, camera values, and tie points are also required before any type of processing can occur.

1.   Aerial Imagery

As the UltraCam Eagle used to collect the WSI imagery is a digital camera this option was chosen. Next, a reference coordinate system was needed; in this case the defaults of a Geographic projection and WGS 84 Datum were left untouched. There are many options for projections and if this information was missing these selections could be left as "unknown." The next piece of required information was the average flying height, in this case 450m.

Once the preliminaries were entered, images could finally be added (right click on "Images" > Add > select from library). More information then had to be included to categorize the interior and exterior orientation of the camera. Specifically the pixel size, perspective center, and rotation angles were needed, which were accessed by right-clicking one of the red boxes under the intended heading.

The next step could have been accomplished in a few different ways. IMAGINE Photogrammetry was programmed to accept both GCPs and/or tie points so as long as enough of one or both were created triangulation could be completed. Clicking on the crosshairs symbol opened the point measurement window. Here both images were viewed simultaneously so that identical points could be created to tie them together. When GPS information was available the point was marked as "Control" in the "Usage" column and the x/y/z values were entered, otherwise it was labeled as "Tie." Once an acceptable number of points were marked, "Automatic Tie Generation" (the symbol looks like a plus sign inside a circle of arrows) was run in order to lessen the workload, although all created tie points had to be checked for accuracy before use. As seen in Figure 21, each point had to be as exact as possible, with zoom windows available to mark them to pixel accuracy.
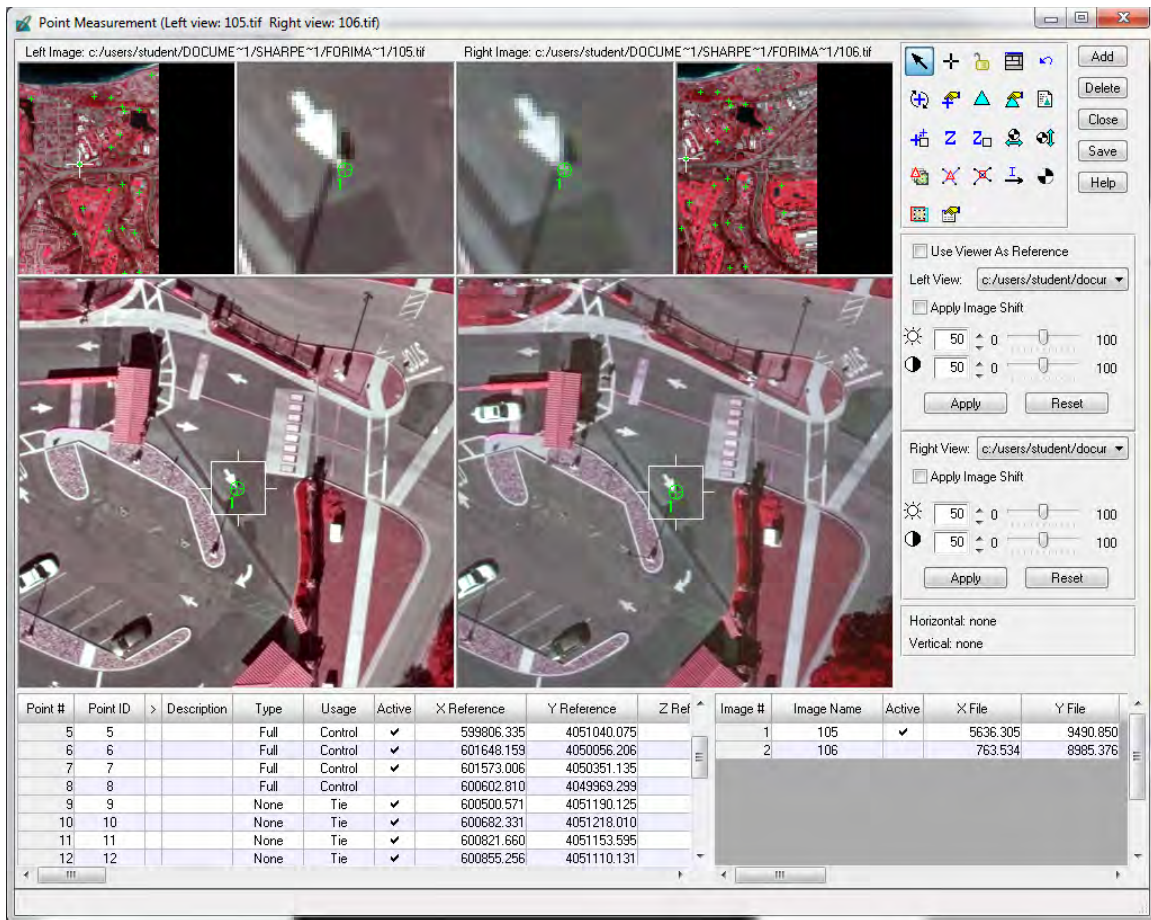
Figure 21.   IMAGINE Photogrammetry's Point Measurement Window

The last step in this window was to "Perform Triangulation" (the blue triangle symbol). This caused the image outlines in the main window to overlap according to their newly determined positions. The images needed to overlap more than 30% for IMAGINE to process them. Figure 22 demonstrates a correctly aligned and marked pair, with GCPs represented as red triangles and tie points shown as red squares.
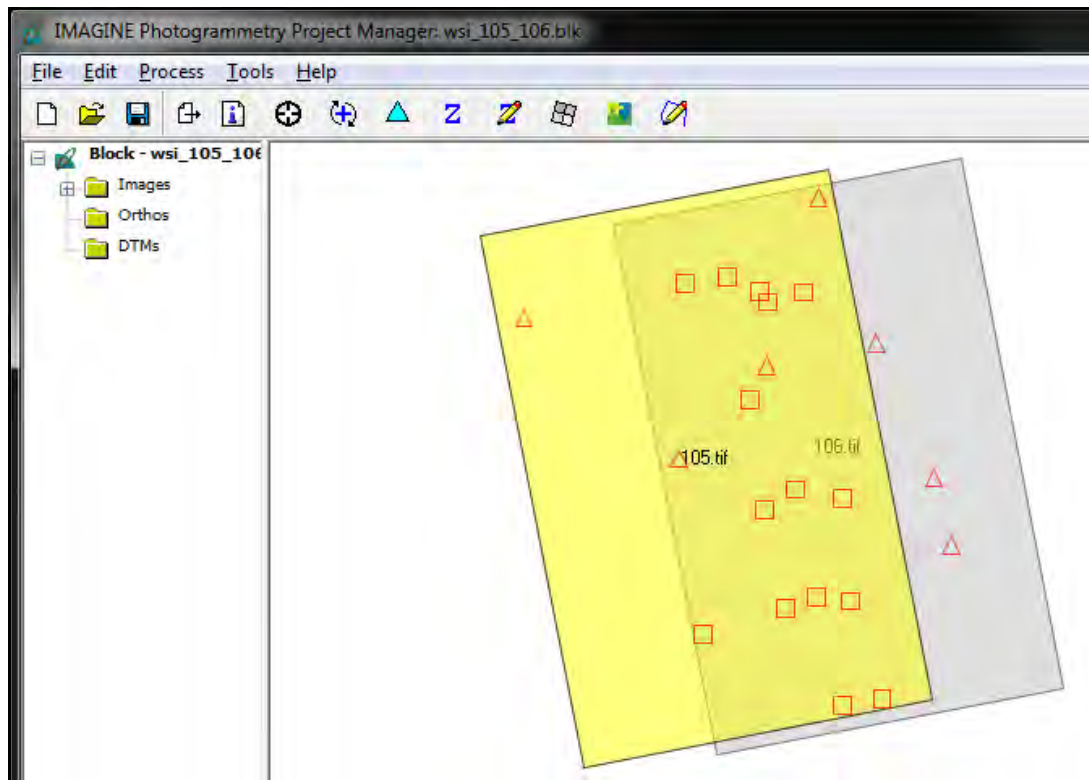
Figure 22.   GCPs and Tie Points in IMAGINE Photogrammetry

Finally, the actual photogrammetry could be completed. The blue "Z" symbol seen at the top of Figure 22 is the "DTM Extraction" tool, from which "eATE" was selected as the preferred method. In the eATE Manager window the last two steps were to click "Generate Processing Elements" (from the Process tab), which highlighted the overlapping area between the images, followed by "Batch Run eATE…" (also under the Process tab) and clicking the "Run Now" button. Depending on the size of the images, final processing took from 30 minutes to hours to complete. The result obtained by entering two of the WSI images can be seen in Figure 23. In spite of doing a fair job of outlining most of the major features, this model is quite lean. Points along color boundaries appear to have been the easiest to associate, indicating the algorithm searches for unique color features to match between the two images. The top portion of Figure 23, a horizontal view of the model, reveals that most of the points represent surfaces at a believable range of elevations, a good portion of them existing on the ground and several others at the levels of trees and building roofs (green and white, respectively).
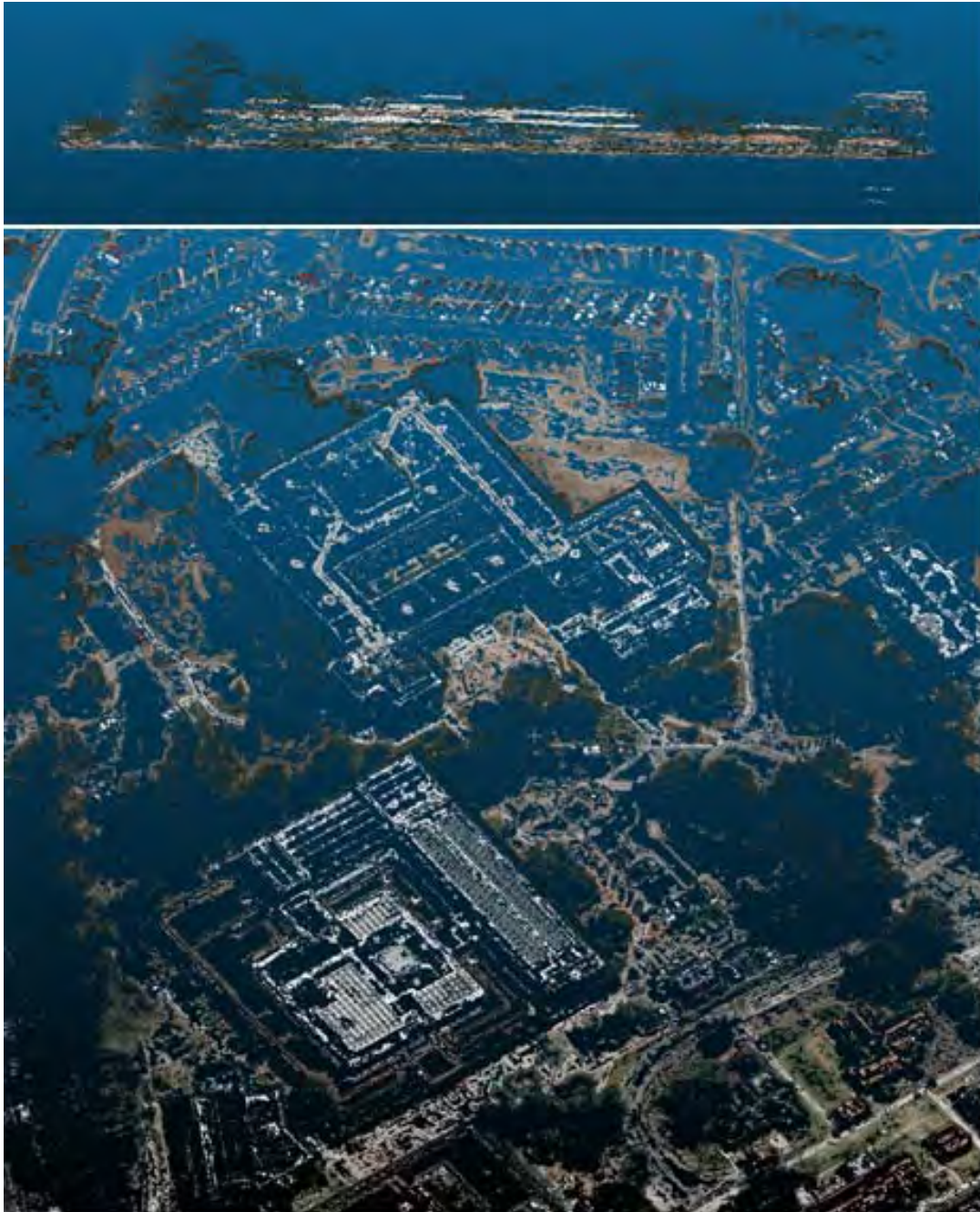
Figure 23.   Photogrammetry Point Cloud of Glasgow Hall, Aerial Imagery

2.   Satellite Imagery

Setting up the Photogrammetry module with satellite imagery was much faster than with aerial imagery because the only information that had to be manually entered was the camera/satellite type and the correct projection and datum. Because all of the

auxiliary information for satellite images is included within rational polynomial coefficient (RPC) files or provided NTFs, all that was necessary was to select the preferred photogrammetry method and run it.

In keeping with the results found in the aerial imagery MVS section, it was decided to use two images from the same satellite for this experiment. This limited the choice to three IKONOS images or two Worldview images, the latter of which did not provide enough overlap. Upon examination, the 2000 November 28 #1 image and the 2002 October 29 image were chosen; they can be seen in Table 3. IKONOS images are provided as NTFs so after specifying the sensor type and Universal Transverse Mercator (UTM) projection of Zone 10, with a World Geodetic System 1984 (WGS 84) datum the manual work was concluded by selecting and running the eATE method.

Figure 24 reveals the panchromatic photogrammetric model created of the Monterey Peninsula. Similar to the aerial result, this model appears to have registered points lying on color boundaries the best, such as roads and buildings. The top view of the figure reveals the elevation changes detected by the model, which generally match the elevations indicated by the red line running through the topographic map to the left.
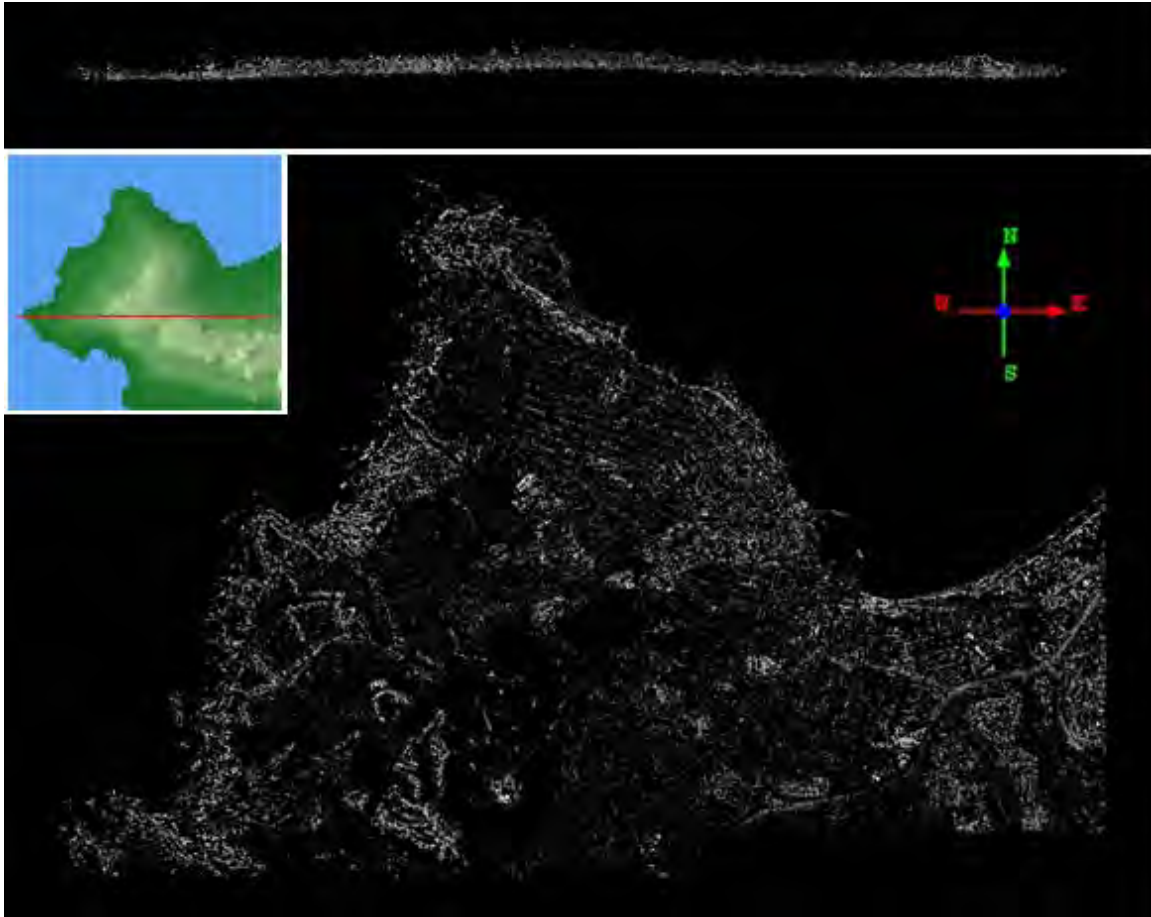
Figure 24.   Stereo Photogrammetry Point Cloud of Monterey, CA; Horizontal
View of the Southern Edge (Top), Topographic Map (Left, after
"Digital Wisdom," 2014), Nadir View (Bottom)

D.   COMPARISON WITH LIDAR

Turning to the CloudCompare software, the LiDAR, IMAGINE, and Agisoft models were opened simultaneously and aligned. Using the LiDAR point cloud as ground truth for the location of objects and buildings, the photogrammetric and MVS datasets were translated and rotated to match. Tables 12 through 16 demonstrate the differences between the three point clouds from different points of view. The first window of each table demonstrates how difficult it was to determine differences between the color models. To solve this problem, the points of the photogrammetric point cloud were changed to purple and those of the MVS point cloud were rendered in yellow with the LiDAR points in white or left as true color.

1. Aerial

The overall meagerness of the photogrammetry point cloud made finding matches between models problematic because the IMAGINE software identified edges of objects but failed to render any kind of homogenous areas such as concrete roads or parking lots, dirt, grass, or building roofs. In Table 12, the main takeaway is that none of the roof points extend into the "shadow" of the wall on the south or west sides of Glasgow Hall. In Table 13, it becomes apparent that the photogrammetry model contains the Glasgow building but it is shifted to the northeast. This can be explained by a characteristic of aerial photography known as relief displacement. This geometric distortion is due to elevation changes and is particularly disturbing in urban areas with tall buildings. Because stereo photogrammetry only makes use of two images it is not surprising this distortion appears in the 3D model.

There is slightly more to be said of the MVS model, in that the entire shape of the building hugs that of the LiDAR model, to include segments of wall on all sides. There are a few dissimilarities seen in the concavities of the building where the MVS model has rounded some of the surfaces instead of providing straight edges, but at least the walls are present.
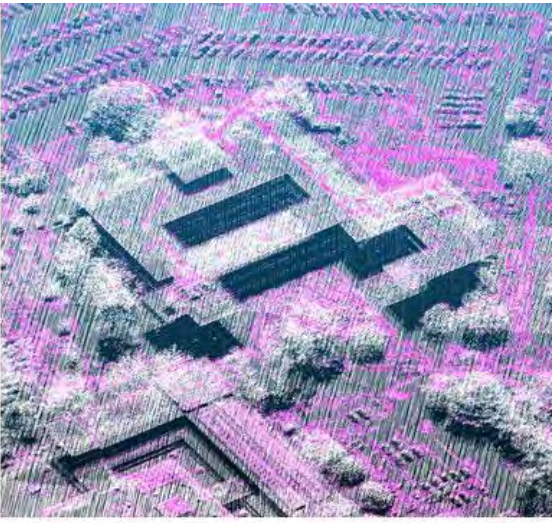
Table 12. Comparing Imagery Results to LiDAR Ground Truth
(View of Glasgow Hall from the Southwest)
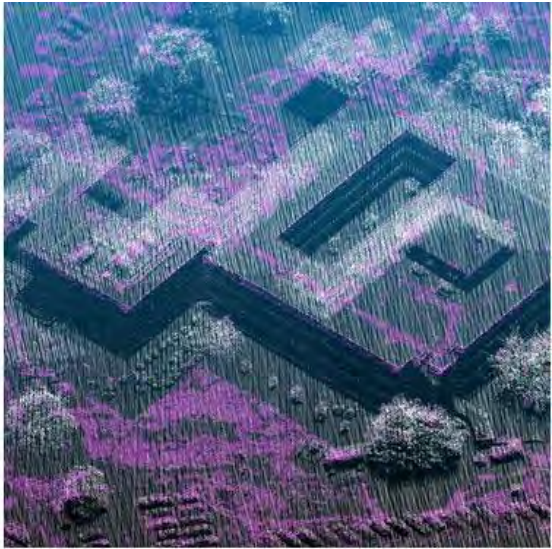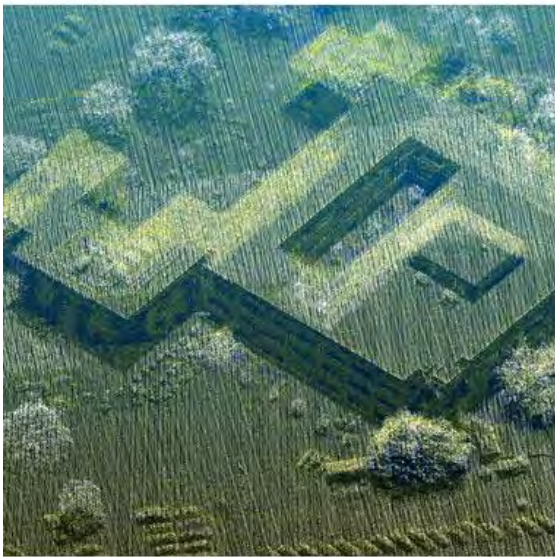
Table 13. Comparing Imagery Results to LiDAR Ground Truth
(View of Glasgow Hall from the Northeast)

Transects of the images seen in Figure 25 demonstrate how closely photogrammetric and MVS models follow the surface of the LiDAR data. The points delineating the ground closely overlap with little to no deviation between the three models. Where vegetation is present the photogrammetric and MVS points outline the

highest points to within half a unit which is reasonable when considering the difficulty of matching leaves and branches between images. Examination of the lower transect revealed the mass of white LiDAR points to the left side of the image, circled in red, was the site of a tree that had been removed between the LiDAR and imagery collections. This explains why no yellow MVS points exist over this spot while there are several along the ground. The few purple points floating above this area are artifacts.

When comparing the structure of the building, the LiDAR and MVS roof points overlap neatly while the few photogrammetric points deviate by half a unit both above and below the LiDAR ground truth. The photogrammetric model is also found lacking where vertical walls are concerned as points are absent along the walls. The downfall of the MVS model is corners and building edges. At the coordinates (80, 10) of the upper view of Figure 25 the center cutout of Glasgow reveals a curved surface. This inner wall differs from the LiDAR by less than half a unit until it reaches the ground where it diverges upward and abruptly stops, fluctuating from the LiDAR by two units. At (70, 26) of the lower view the MVS model rounded the upper roof, differing by half a unit in both the x and y directions.
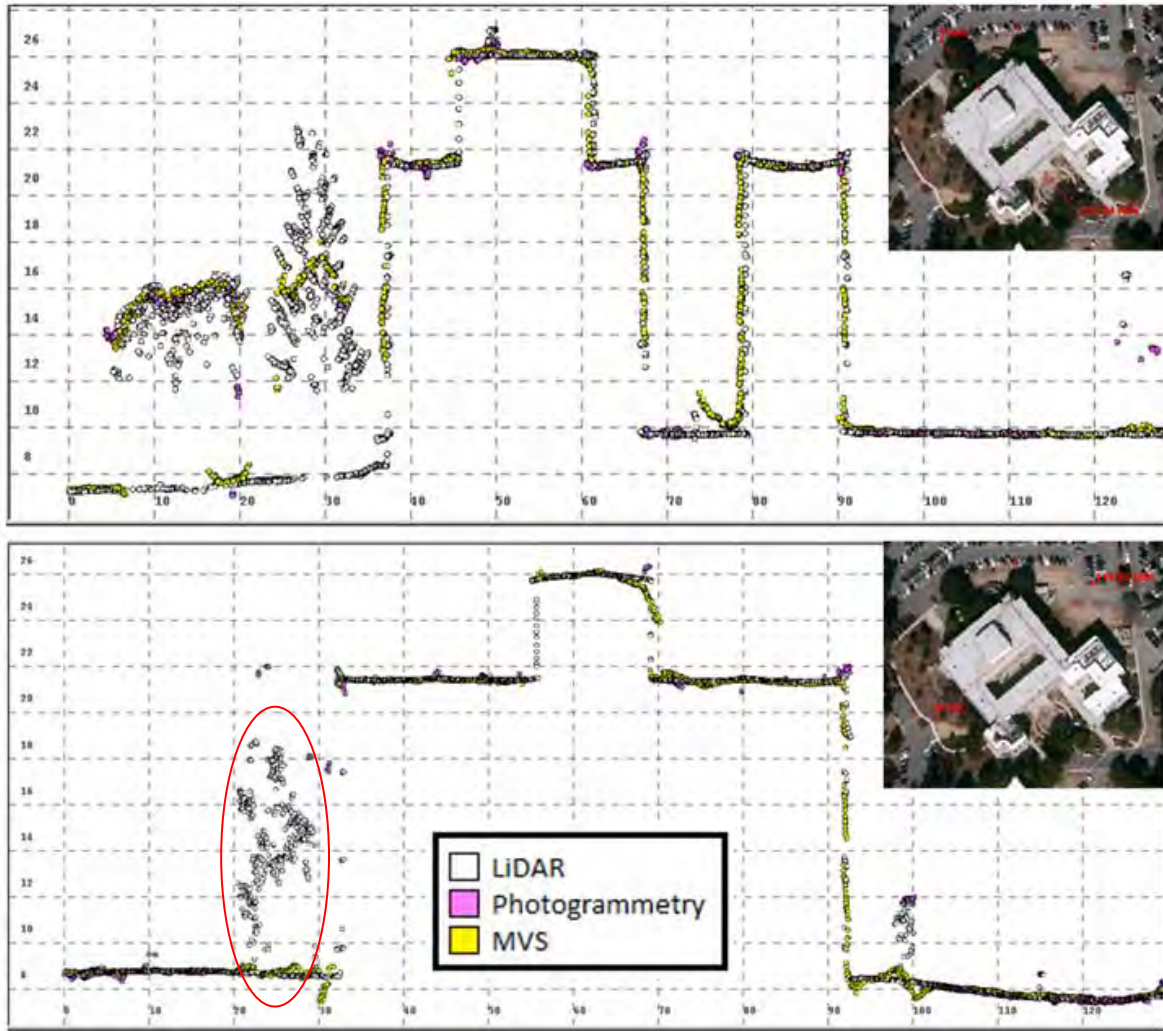
Figure 25.   Transects of Glasgow Hall Models Using Aerial Imagery, Top:
Northwest to Southeast, Bottom: Southwest to Northeast

2.   Satellite

For this section, both the photogrammetric and MVS satellite models were clipped to the same size around the NPS campus. Figures 26 and 27 demonstrate the point densities of each method, with the photogrammetric model again showing a reliance on color boundaries while the MVS model is much more inclusive.
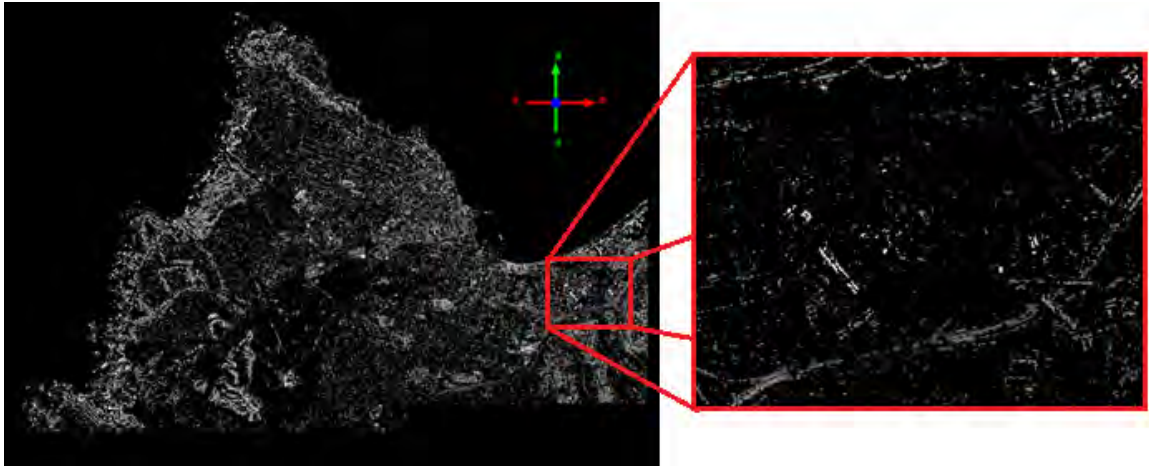
Figure 26.   Aerial Photogrammetry Model of Monterey, Clipped to NPS
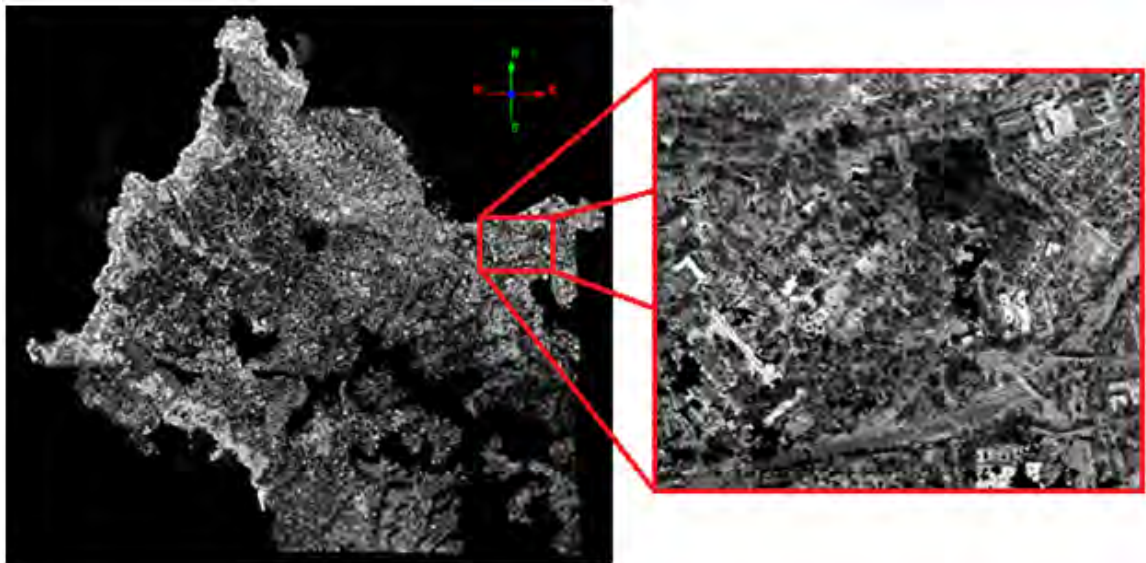
Figure 27.   MVS Satellite Model of Monterey, Clipped to NPS

Due to the much higher density of the LiDAR point cloud, it was not meaningful to render the points in white for the comparisons shown in Figures 28 through 31, so the LiDAR data was left in true color. The photogrammetry model was changed to red or purple and the MVS model was rendered in yellow to make visual analysis easier.

The results from the automated photogrammetric analysis were disappointing. Photogrammetric approaches can clearly produce better results, but more human intervention may be required. As seen in Figure 28, the red points of the photogrammetry

model loosely match the LiDAR data. It was difficult to align the two models because of the sparse number of photogrammetry points but the highway was used as a constant across the 12-year span between datasets. Once the road had been lined up the lack of coherence between man-made structures became quite obvious as the photogrammetry model failed to outline buildings and only a few continuous surfaces can be found. The eATE module of IMAGINE Photogrammetry was utilized both with and without manually entered tie points in hopes of improving the result but the outcomes were nearly identical. The unexpectedly poor result may be due to the temporal span between the satellite images which is nearly two years. Other factors may include the method of output, as .las files are not usual photogrammetric products.

The MVS model seen in Figure 29 covers more features than the photogrammetry model but only about half of it is visible. After a mean ground level had been identified within the MVS model, it was aligned with the LiDAR and about 50 percent of the points fell below said level. This is more clearly demonstrated in Figures 30 and 31. The vertical errors of the two models are equally poor, indicating neither should be utilized further unless corrections are made.
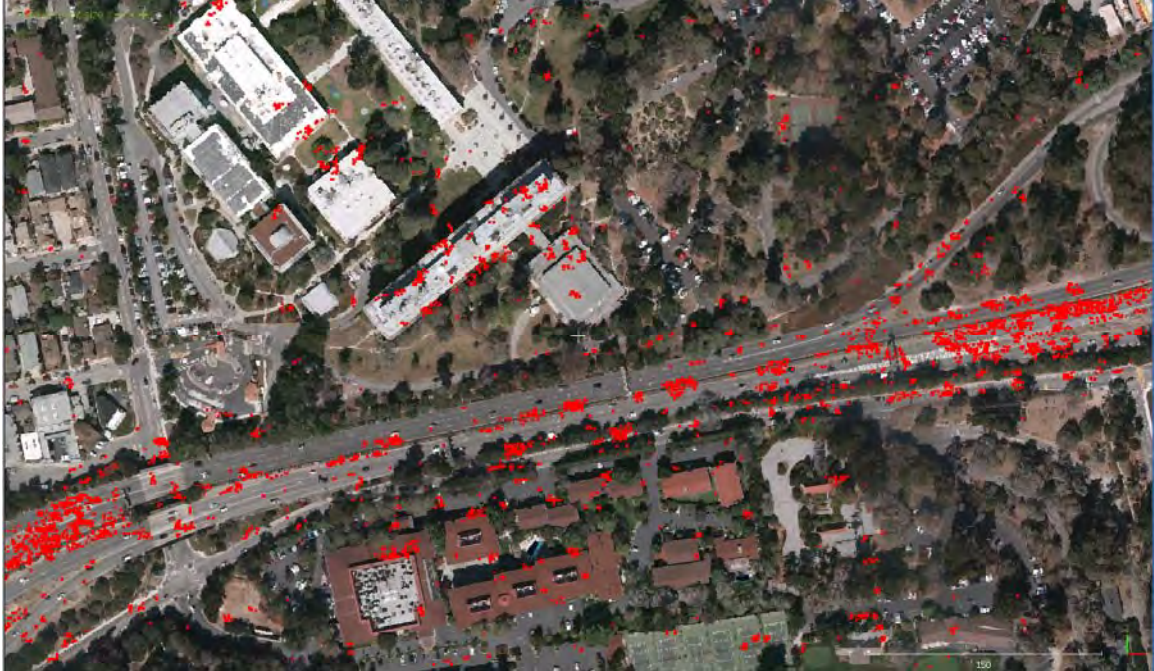
Figure 28.   Close-up of Satellite Photogrammetry Model with LiDAR of NPS

Figure 29.   Close-up of Satellite MVS Model with LiDAR of NPS

Figure 30.   Horizontal View of Satellite Photogrammetry Model with LiDAR of NPS
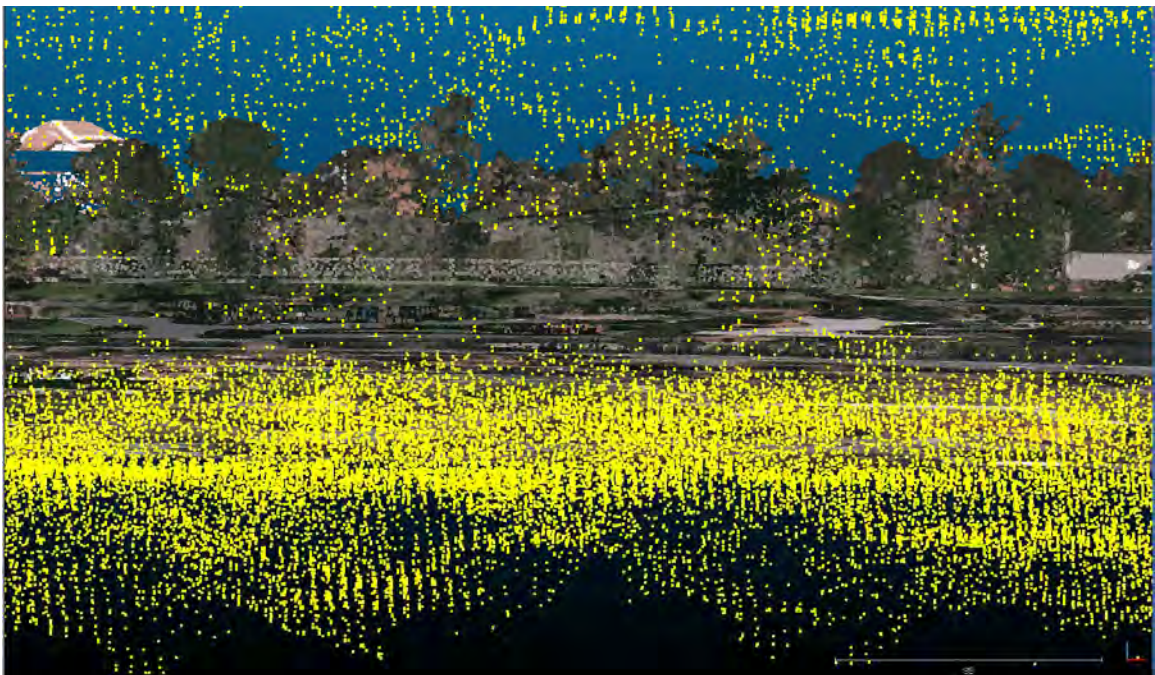
Figure 31.   Horizontal View of Satellite MVS Model with LiDAR of NPS

Figure 32 more clearly illustrates the inconsistent elevation values provided by the photogrammetry and MVS software. The purple points range as far as 100 units from the LiDAR data and the yellow points range as much as 80 units, confirming the software packages were not meant to handle satellite data.
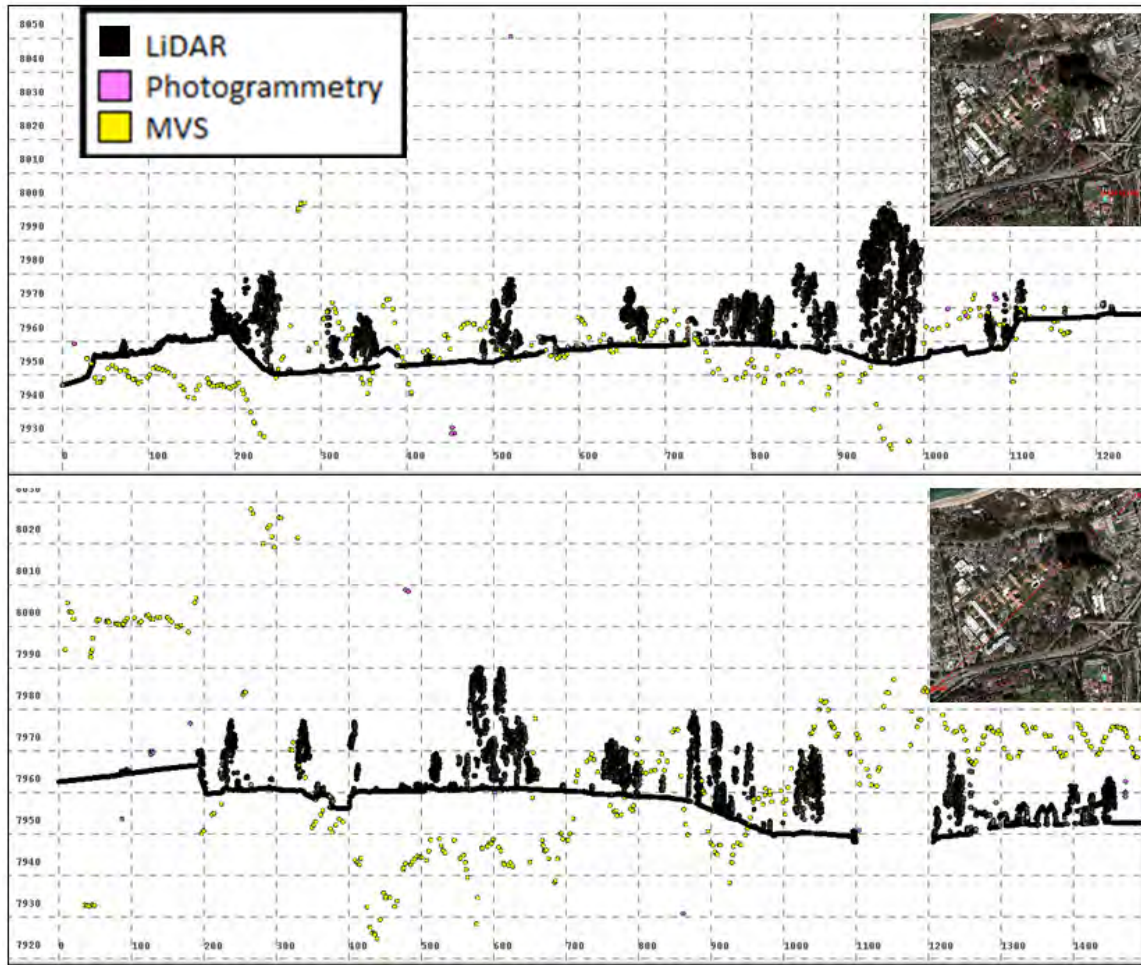
Figure 32.   Transects of Glasgow Hall Models Using Satellite Imagery, Top: Northwest to Southeast, Bottom: Southwest to Northeast

THIS PAGE INTENTIONALLY LEFT BLANK

V.   SUMMARY AND CONCLUSION

This research revealed the capabilities of two software packages in creating point cloud models from both aerial and satellite imagery. Images included those taken with Hasselblad and UltraCam Eagle digital cameras as well as four satellites: IKONOS, Worldview-1, Quickbird-1, and GeoEye-1. A LiDAR dataset collected by WSI at a point density of 30 points/m^2 constituted the ground truth which the imagery point clouds were measured against.

In the aerial imagery MVS trials it was found that when combining three different datasets of the same location, Glasgow Hall on the NPS campus, the best model was not necessarily the one with the most images. A single dataset, six photographs collected by WSI, that provided unique views produced a more complete model of Glasgow Hall than the combined model with twelve images. It was determined in the third trial that within a single image dataset results improve when more images are included.

The satellite imagery MVS trial was less conclusive as there were only seven available images of the Monterey Peninsula from four satellites offering different resolutions. The results indicated that improvements occurred between each run without any obvious digression so further work must be completed to determine the ideal number of satellite images to be included.

On the photogrammetry side, the aerial imagery produced very accurate results. While some relief displacement occurred due to the angles of the two images used and holes existed anywhere homogenous surfaces disallowed point registration, the points that were created as part of this model represented the most truthful elevation values. Unlike the MVS aerial model which rounded some of the buildings' walls, the photogrammetry point cloud stayed true to shape.

When comparing the satellite photogrammetric and MVS models it was found that neither was accurate enough to use at present. Viewing them horizontally, the MVS model registered the most points by far while the photogrammetric model contained so few points it was difficult to identify anything other than a stretch of road and a few

building roofs. The spread of z values was so high in both models we conclude these software packages were not created to work with satellite data as their vertical data were invalid.

According to these tests LiDAR remains the model of choice due to its accurate elevation values. Software packages utilizing aerial imagery have improved to the point that models indicating the general shape and location of objects are possible, even including building walls and vertical structures. On the other hand, satellite imagery products require more rigorous algorithms to ground points to surfaces before they can be of further use.

Subsequent research should focus on overcoming software weaknesses in analyzing satellite imagery. If vertical data could be correctly determined, satellite models could be used to represent much larger areas in less time. Further research into other software packages might also reveal capabilities not found in those studied here.

LIST OF REFERENCES

Aerial Photography. (2013). In J. Hannavy (Ed.), *Encyclopedia of nineteenth-century photography* (p. 13). London: Routledge.

Agarwal, S., Furukawa, Y., Snavely, N., Simon, I., Curless, B., Seitz, S. M., & Szeliski, R. (2011). Building Rome in a day. *Communications of the ACM,* 54(10), 105–112. doi: 10.1145/2001269.2001293

Bagley, J. (1917). *The use of the panoramic camera in topographic surveying.* Washington DC: Government Printing Office.

Basgall, P. (2013). *LiDAR point cloud and stereo image point cloud fusion* (master's thesis). Retrieved from Calhoun: http://hdl.handle.net/10945/37584

Church, E., & Quinn, A. (1948). *Elements of Photogrammetry*. Syracuse, NY: Syracuse University Press.

Diaz, J. C. F. (2011). Lifting the Canopy Veil: Airborne LiDAR for Archaeology of Forested Areas. *Imaging Notes,* 26(2) , 31–34.. Retrieved from http://www.imagingnotes.com/go/article_freeJ.php?mp_id=264

Digital Wisdom [Image]. (2014). Retrieved from https://www.digiwis.com/dwi_uss.htm

Digital Globe. (2013). Data sheets for IKONOS, GeoEye-1, Worldview-1, and Quickbird 2. Retrieved from http://www.digitalglobe.com/resources/satellite-information

Dismukes, K. (2005). Space Shuttle basics, human space flight. Retrieved from http://spaceflight.nasa.gov/shuttle/reference/basics

Early Techniques and Equipment [Image]. (2000). Retrieved September 5, 2014 from https://airandspace.si.edu/exhibitions/looking-at-earth/online/script/ss_early2.htm

Eisert, P., Steinbach, E., & Girod, B. (1999). Multi-hypothesis, volumetric reconstruction of 3-D objects from multiple calibrated camera views. In *Proceedings of the 1999 IEEE International Conference on Acoustics, Speech, and Signal Processing,* 6, pp. 3509–3512. IEEE. doi: 10.1109/ICASSP.1999.757599

Erdkamp, J. (2011). Theodor Scheimpflug: The life and work of the man who gave us that rule. *Photohistorisch Tijdschrift/Photo-Historical Journal,* 34,3. Retrieved from http://kodaksefke.eu/scheimpflug-file.html

Erdkamp, J. (2011). The Theodor Scheimpflug file. Retrieved from http://kodaksefke.eu/scheimpflug-file.html.

Faugeras, O., & Keriven, R. (2002). Variational principles, surface evolution, PDE's, level set methods and the stereo problem. In *Proceedings of the 5th European Conference on Computer Vision,* pp. 379–393. doi: 10.1109/SSBI.2002.1233990

Furukawa, Y., & Ponce, J. (2010). Accurate, dense, and robust multiview stereopsis. *IEEE Transactions on Pattern Analysis and Machine Intelligence,* 32(8), pp. 1362–1376. doi: 10.1109/TPAMI.2009.161

Gargallo, P., & Sturm, P. (2005). Bayesian 3D modeling from images using multiple depth maps. In *Proceedings of the IEEE Computer Society Conference on Computer Vision and Pattern Recognition,* 2, pp. 885–891. IEEE. doi: 10.1109/CVPR.2005.84

Guerra, F., & Pilot, L. (2000). Historic photoplanes. In *International Archives of Photogrammetry and Remote Sensing,* XXXIII(B5), 611–618. Retrieved from http://www.isprs.org/proceedings/xxxiii/congress/part5/611_XXXIII-part5.pdf

Hartley, R. I., & Mundy, J. L. (1993). The relationship between photogrammetry and computer vision. In *Optical engineering and photonics in aerospace sensing,* pp. 92–105. International Society for Optics and Photonics.

Hirschmuller, H. (2005). Accurate and efficient stereo processing by semi-global matching and mutual information. In *Proceedings of the IEEE Computer Society Conference on Computer Vision and Pattern Recognition,* 2, pp. 807–814. IEEE. doi: 10.1109/CVPR.2005.56

Hirschmüller, H. (2011). Semi-global matching motivation, developments and applications. *Photogrammetric Week*, 53, 173–184. Retrieved from http://www.ifp.uni-stuttgart.de/publications/phowo11/180Hirschmueller.pdf

Image-based measurements in machine vision: technology hints [Image]. (2008). Retrieved from http://cvg.deis.unibo.it/technology_hints_en.html

Laussedat, Aimé. (1899). La Métrophotographie. Paris, France: Gauthier-Villars, Imprimeur-Libraire. Retrieved from http://becot.info/opus/analecta/Laussedat_Metrophotographie1899.pdf

Laussedat, Aimé. (2008). In *Complete dictionary of scientific biography*. Retrieved from http://www.encyclopedia.com/doc/1G2-2830902500.html

Lindeberg, T. (2012). Scale invariant feature transform. In *Scholarpedia.* Retrieved from http://www.scholarpedia.org/article/Scale_Invariant_Feature_Transform# Extensions

Merklinger, H. (1996). Scheimpflug's patent. *Photo Technique.* Retrieved from http://www.trenholm.org/hmmerk/HMArtls.html

Moffitt, F. (1959). *Photogrammetry.* Scranton, PA: International Textbook Company.

Morris, D., & Kanade, T. (2000). Image-consistent surface triangulation. In *Proceedings of the IEEE Computer Society Conference on Computer Vision and Pattern Recognition,* 1, pp. 332–338. IEEE. doi: 10.1109/CVPR.2000.855837

NPS Statistics [Image]. (2014). Retrieved from www.nps.edu/About/NPS_Statistics

Old Delft Scanning Stereoscope [Image]. (2009). Retrieved from http://www.publicsurplus.com/sms/auction/view?auc=310310

Quam, L. H. (1971). *Computer comparison of pictures* (No. STAN-CS-71-219). Stanford Univ CA Dept Of Computer Science. Retrieved from http://www.dtic.mil/cgi-bin/GetTRDoc?AD=AD0785172

Rosenfeld, A. (1969). Picture processing by computer. *ACM Computing Surveys (CSUR),* 1(3), 147–176. doi: 10.1145/356551.356554

Saiz, Angel. (2012). Nadar. Retrieved from http://historiasdearteyguerra.blogspot.com/2012/09/nadar.html

Schuckman, K., & Renslow, M. (2014). *Ground-based platforms.* Pennsylvania State University: John A. Dutton e-Education Institute. Retrieved from https://www.e-education.psu.edu/lidar/l2_p5.html

Seitz, S. M., Curless, B., Diebel, J., Scharstein, D., & Szeliski, R. (2006). A comparison and evaluation of multi-view stereo reconstruction algorithms. In *IEEE Computer Society Conference on Computer vision and pattern recognition,* 1, pp. 519–528. IEEE. doi: 10.1109/CVPR.2006.19

Seitz, S. M. & Dyer, C. R. (1999). Photorealistic Scene Reconstruction by Voxel Coloring. *International Journal of Computer Vision,* 35(2), pp. 151–173. doi: 10.1023/A:1008176507526

Shan, J., & Toth, C. K. (2009). *Topographic laser ranging and scanning: Principles and processing.* Boca Raton, FL: CRC Press/Taylor & Francis Group.

Shepherd, E. (2006). Il rilievo topofotografico di Ostia dal pallone 1911. In *Archeologia Aerea Studi di Aerotopografia Archeologica,* 2, pp. 15–38. Retrieved from http://www.ostia-antica.org/fulltext/shepherd/shepherd_aaerea.pdf

Tardivo, C. (1911). *Manuale di fotografia-telefotografia, topofotografia dal pallone.* Torina.

Total station and its applications in surveying [Image]. n.d. Retrieved September 3, 2014 from http://www.gisresources.com/total-station-and-its-applications-in-surveying

University of Texas at Austin (2013). *Monterey Naval Postgraduate School Data Collect.* Austin, TX: University of Texas.

Van Gool, L., Tuytelaars, T., Ferrari, V., Strecha, C., Wyngaerd, J. V., & Vergauwen, M. (2002). 3D modeling and registration under wide baseline conditions. *International Archives of Photogrammetry and Remote Sensing,* 34(3A), 3–14.

Watershed Sciences, I. (2012). *Monterey Naval Postgraduate School Data Collect.* Portland, Oregon: Watershed Sciences, Inc.

Walker, S. (2007). New features in SOCET SET®. *Photogrammetric Week*, 49(7), 35–40. Retrieved from http://www.ifp.uni-stuttgart.de/publications/phowo07/060Walker.pdf

INITIAL DISTRIBUTION LIST

1.   Defense Technical Information Center
        Ft. Belvoir, Virginia

2.   Dudley Knox Library
        Naval Postgraduate School
        Monterey, California